Functional characterization of the ligand binding properties of the Atlantic cod (*Gadus morhua*) peroxisome proliferator-activated receptor a1 and a2

By Kristianne Hjorth Viken

Thesis submitted in partial fulfilment of the requirements for the degree of Master of Science

Department of Biological Sciences

Faculty of Mathematics and Natural Sciences

University of Bergen

September 2020

ACKNOWLEDGEMENTS

This study has been part of the iCod 2.0 project (project no. 244564) and dCod 1.0 project funded by the Research Council of Norway (project no. 248840) as part of the Digital Life Norway initiative.

First, I would like to thank my main supervisor Odd André Karlsen for introducing me to the topic of environmental toxicology in my bachelor's degree and, allowing me to also do my thesis in environmental toxicology. Thank you for always helping me by answering my questions, and being very interested in all of my results, preferably the day when they are ready. I also really appreciate all the help you have given me in the writing process. I would also like to thank my co-supervisor Anders Goksøyr for helping me in the writing process, your interest in the topic of science and toxicology is inspirational.

Next, my biggest gratitude goes to my other co-supervisor Roger Lille-Langøy for teaching me so much in the lab, always having a solution for everything. The hours I have spent with you both in the lab and in your office, I think is countless, I appreciate that very much.

This whole year has been such an experience which I am thankful for. The environment at UiB has been amazing and supporting. A big thanks also to my fellow students both at EnvTox and Mol for support, encouragement and long lunches. I would also like to thank my family and friends for always supporting me and showing interest in this molecular biology, although you might not understand very much of it. Last special thanks to Eivind, for always supporting and believing in me.

Bergen, September 2020

Kristianne Hjorth Viken

TABLE OF CONTENTS

SELECTED ABBREVIATIONS

BSA	Bovine serum albumin
β-ME	beta-mercaptoethanol
β-gal	beta-galactosidase
CFDA-AM	5-carboxyfluorescein diacetate acetoxymethyl ester
DBD	DNA binding domain
DDT	Dichlorodiphenyltrichloroethane
DMEM	Dulbeccoś Modified Eagle´s Medium
DMSO	Dimethyl sulfoxide
DTT	DL-Dithiothreitol
EC_{50}	Half maximal effective concentration
EDTA	Ethylenediaminetetraacetic acid disodium salt dehydrate
EGTA	Ethylene glycol-bis(2-aminoethylether)-N,N,N´, N´-tetraacetic acid
E_{max}	Maximal effect
FA	Fatty acid
FBS	Fetal Bovine Serum
gmPpara	*Gadus morhua* Ppara
LB	Lysogeny broth
LBD	Ligand-binding domain
LRA	Luciferase reporter gene assay
MSA	Multiple sequence alignment
NR	Nuclear receptor
ONPG	Ortho-2-Nitrophenyl-β-D-galactopyranoside
ONP	o-nitrophenol
PBS	Phosphate-buffered saline
PFASs	Perfluorinated alkylated substances
PFHxS	Perfluorohexanesulfonic acid
PFNA	Perfluorononanoic acid
PFOA	Perfluorooctanoic acid
PFOS	Perfluorooctanesulfonic acid
PMSF	Phenylmethanesulfonyl fluoride
PPARs	Peroxisome proliferator-activated receptors
RXR	Retinoid X receptor
SDS-PAGE	Sodium dodecyl sulphate polyacrylamide gel electrophoresis
SOC	Super optimal broth with catabolite repression
UAS	Upstream activation sequence
WT	Wild type
WY-14643	4-chloro-6[(2.3-dimethylphenyl)amino]-2-pyrimidinyl]thio-acetic acid (Pirinixic acid)

ABSTRACT

Perfluoroalkylated substances (PFASs) are persistent in nature, resisting both biotic and abiotic degradation, resulting in the bioaccumulation of these substances in organisms, as well as biomagnification upwards the trophic levels in both terrestrial and marine food webs. These properties has made PFASs an environmental concern.

The peroxisome proliferator-activated receptors (PPARs) are ligand-activated transcription factors and members of the superfamily of nuclear receptors. The PPAR subfamily consists of three members: PPARa, PPARd, and PPARg. The different subtypes have distinct roles in the regulation of the lipid homeostasis, differing in tissue specific expression, ligand specificity, and target genes. Atlantic cod (*Gadus morhua*) has four different gmPpars; gmPpara1, gmPpara2, gmPpard and gmPparg. gmPpara1 has been demonstrated to be activated by some exogenous compounds including the PPARa model-agonist WY-14643, and four PFASs, including PFOA, PFNA, PFHxA, and PFHxS. Although the gmPpara2 subtype is also responsive to WY-14643, it is not activated by any of the PFASs. When aligning the protein sequence of gmPpara1 and gmPpara2, an extension of 14 additional amino acids (AAs) in the hinge region of gmPpara2 is observed. Moreover, two AAs important for the binding of WY-14643 in a second allosteric binding site identified in the human ortholog (hPPARa) differ in gmPpara2 compared to gmPpara1. We hypothesized that these differences play a role in the observed discrepancies in the activation profiles of gmPpara1 and gmPpara2.

In this study, site-directed mutagenesis was used to remove the 14 additional AAs in the hinge region, and mutate the two AAs in the putative second binding site in gmPpara2. A luciferase-based reporter gene assay in COS-7 cells was then used to study ligand activation of the gmPpars (wild types and mutants) when exposed to WY14643 and selected PFASs. Protein immunoblotting were used to confirm the synthesis and presence of the gmPpar variants in the COS-7 cells, and a cytotoxicity assay was used to monitor the cytotoxicity of the ligands.

Four different mutants were successfully constructed. Notably, the removal of the 14 AAs in the hinge region had a large impact on the activation profile with WY-14643, producing a 15 and 6 times higher fold activation in comparison to the wild type gmPpara2, and gmPpara1, respectively. Mutants containing the AA substitutions in addition to the deletion also increased the WY-14643-mediated activation, but slightly less compared to the gmPpar variant containing only the 14 AA deletion. Intriguingly, none of the mutants were activated by any of the three PFASs tested.

1. INTRODUCTION

1.1 PERFLUOROALKYLATED SUBSTANCES (PFAS)

In the later years, a concern about fluorinated compounds, and especially perfluoroalkylated substances (PFAS), has emerged (Fàbrega, Kumar, Schuhmacher, Domingo, and Nadal (2014)). In Norway, PFAS have especially been accentuated in the media recently because of how such compounds are used as functional components of ski wax used in cross-country skiing and biathlon. However, these substances have now been banned from use in international competitions. PFASs are not newly synthesized chemicals, but have been produced and manufactured for over 60 years. PFASs have been widely used in a variety of applications in both the industries and in consumer products, including water-repellent fabrics, fire-fighting foams, non-stick surfaces in cooking pans, and as lubricants, among others (Fàbrega et al., 2014). In general, PFAS molecules usually have a carbon-backbone of variable length, where fluorines have substituted the hydrogen atoms. On one of the ends they usually have a functional group, such as a carboxyl- or sulfonate group. This makes PFASs amphipathic, where the carbon backbone constitutes the hydrophobic part, and the functional group adds hydrophilicity to the molecules (Fàbrega et al., 2014; Fujii, Polprasert, Tanaka, Hong Lien, & Qiu, 2007). Currently, the most widely used PFAS molecule is perfluorooctanesulfonic acid (PFOS), consisting of an eight carbon-backbone and sulfonate as its functional group, followed by perfluorooctanoic acid (PFOA), which possesses a seven carbon backbone and a carboxyl group (Fujii et al., 2007). These PFASs, together with perfluorononanoic acid (PFNA), which has a nine carbon backbone and a carboxyl group (Jantzen, Annunziato, Bugel, & Cooper, 2016), have been studied in this thesis (Fig. 1.1).

PFASs have shown to be persistent in the environment, resisting both biotic and abiotic degradation. This makes PFASs accumulate in nature, where they are prone to long transportation by atmospheric circulation and ocean currents. It appears as the majority of released PFASs end up in the oceans, potentially posing a threat to marine species and ecosystems (Prevedouros, Cousins, Buck, & Korzeniowski, 2006). Here, the PFASs can bioaccumulate in organisms, and biomagnify upwards the trophic levels (Boisvert, Sonne, Rigét, Dietz, & Letcher, 2019; Simonnet-Laprade et al., 2019). PFASs have been detected in

remote areas, including the Arctic where it is released from atmospheric deposition and transportation by ocean currents. The presence of PFAS in the Arctic has been documented by its detection in several organisms living there (Muir et al., 2019).

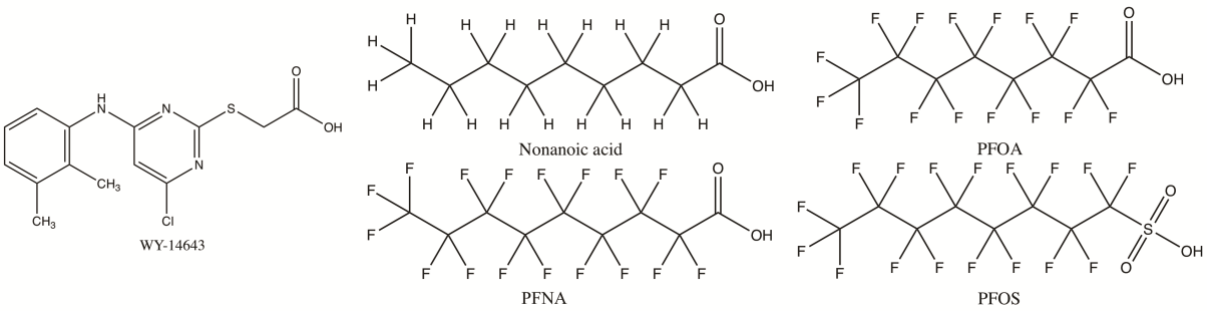

Figure 1.2: Structures of nonanoic acid, WY14643, and selected PFASs. The structures of WY-14643, nonanoic acid (saturated fatty acid), PFOA, PFNA and PFOS are shown as indicated. Structures were found at Chemspider and drawn with ChemDraw.

In 2008/2009 samples of Atlantic cod from 15 Norwegian fjords were investigated, and PFASs were detected in cod liver and blood, including PFOA, PFNA and PFOS. Significantly higher levels of PFASs in the eastern fjords compared to the western and northern fjords of Norway were revealed (Valdersnes, Nilsen, Breivik, Borge, & Maage, 2017). PFASs have also been detected in blood samples and liver samples from Atlantic cod living in the Baltic Sea. PFOS and perfluorooctanesulfonamide (PFOSA) were predominating congeners in those samples, but also PFOA and perfluorodecanoate (PFDA) were detected (Falandysz et al., 2007; Schultes, Sandblom, Broeg, Bignert, & Benskin, 2020). Low levels of PFASs have also been detected in halibut (*Hippoglossus hippoglossus*) along the Norwegian coast (Muir et al., 2019).

Since PFASs have emerged as an environmental concern, the most used congeners, including PFOA and PFOS, their salts, and related compounds, have been included in the Stockholm Convention on Persistent Organic Pollutants. Moreover, the Norwegian Environmental Agency has PFASs on their list of prioritized environmental pollutants, which make them included in all surveillance and monitoring programs in Norway. PFOS is also on the OSPARs List for Chemicals of Priority Action (COMMISION, 2019).

1.2 Peroxisome Proliferator-Activated Receptors (PPARs)

The peroxisome proliferator-activated receptors (PPARs) are ligand-activated transcription factors that are members of the superfamily of nuclear receptors (NRs). When PPARs were first discovered in rodents, they were seen as receptors that promote peroxisome proliferation and increased the number of peroxisomes in the cells, hence named peroxisome proliferator-activated receptors (I. Issemann & S. Green, 1990). Later it was discovered that PPARs had a broader functional role than just proliferating peroxisomes. PPARs are also involved in other physiological processes, such as cell differentiation, development, and importantly, as a key regulator of the lipid and energy homeostasis (Dreyer et al., 1992; Isabelle Issemann & Stephen Green, 1990).

PPARs are divided into three subtypes, PPARa (NR1C1), PPARd (NR1C2) and PPARg (NR1C3) (Hong, Xu, & Zhai, 2018). The sub-types have different physiological roles in the energy metabolism and fat storage, which also include tissue specificity and target gene repertoire (Fig.1.2). The PPARs are mainly found in metabolically active tissues, such as heart, kidney, liver and muscle. They sense changes in the dietary lipids and modulate the gene expression of different target genes. In mammalian species it has been shown that PPARa has an essential role in fatty acid (FA) uptake and metabolism, including β-oxidation of FAs. The FA oxidation provides energy to peripheral tissues (Tyagi, Gupta, Saini, Kaushal, & Sharma, 2011). PPARd is also important for FA oxidation, promoting FA metabolism, and suppresses macrophage-derived inflammation. It activates different genes important for β-oxidation and energy dissipation through uncoupling of the mitochondria. PPARd also plays a key role in the cholesterol metabolism (Grygiel-Górniak, 2014; Tyagi et al., 2011). PPARg is involved in energy storage and glucose metabolism, by regulating insulin sensitivity. It is involved in regulating the expression of genes necessary for the differentiation of fibroblasts into adipocytes. Its most widely studied ligand is thiazolidinedione (TZD), which is a drug used to treat type 2 diabetes (Tyagi et al., 2011). Human PPARg can also be activated by derivates of prostaglandins, derivates of FA, and rosiglitazone (Ma, Wang, Zhao, & Xu, 2018).

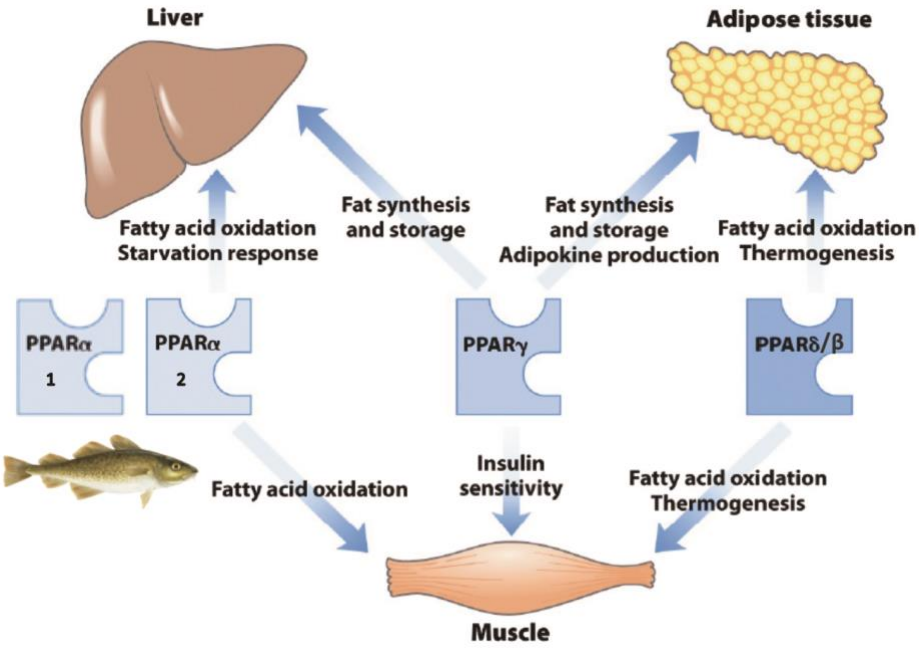

Figure 1.2: Metabolic regulation by the different PPAR subtypes. PPARa, PPARd and PPARg collectively regulate and maintain lipid and glucose homeostasis. In humans, PPARa regulate fatty acid (FA) oxidation in the liver and muscle. PPARg controls fat synthesis and storage in the liver, as well as the insulin sensitivity in the muscles. PPARd also regulates and promotes FA oxidation in muscle, but also in adipose tissues, and regulates thermogenesis. Picture source: (Lehninger et al., 2008). In Atlantic cod there are four different Ppars, as cod possesses two Ppara paralogs in addition to Pparg and Ppard. Hovewer, the exact functions of the Ppar subtypes in teleosts are not yet described.

While the PPARs in humans and rodents are widely studied, much less is known about the exact function of Ppar subtypes in fish. Nevertheless, the Ppars have been cloned from many teleosts, and sequence alignments and phylogenetic analyses have confirmed that the fish Ppars are homologs of the mammalian PPARs (Leaver et al., 2005). In teleost species all three subtypes of Ppars have been identified, but some species possess two paralogs of Ppara, e.g Japanese puffer (*Fugu rubripes*) (Maglich et al., 2003), green spotted puffer (*Tetraodon nigroviridis*) (Metpally, Vigneshwar, & Sowdhamini, 2007), loach (*Misgurnus anguillicaudatus*) (Liang, Gao, Li, & Cao, 2016), zebrafish (*Danio rerio*) (Den Broeder, Kopylova, Kamminga, & Legler, 2015), as well as Atlantic cod (*Gadus morhua*).[1]

[1] In this thesis I follow the nomenclature, where proteins from mammals are written in all capitals ("HGNC Guidelines,"), whereas short names of fish proteins are written with only the first letter in capital (Nathan Dunn, 2019).

1.2.1 Endogenous and exogenous ligands for PPAR

Since the three types of PPARs have different roles in the lipid metabolism and storage, they are also activated by different ligands. In comparison to other NRs, the PPARs ligand binding pocket is 3-4 times larger (1300-1400 Å). This may cause other non-endogenous ligands to bind PPARs with relatively low affinity. The shape of their ligand pocket also determines which ligands they can bind (Xu et al., 2001). The interior of the entrance to the ligand binding site is mainly hydrophobic, in agreement with the hydrophobicity of the natural ligands (Zoete, Grosdidier, & Michielin, 2007). The ligands recognized by PPARa are usually fatty acids and their derivates, like eicosanoids. Exogenous ligands that have been demonstrated to bind PPARa include fibrates, which is used for treatment of hypertriglyceridemia and mixed dyslipidemia (Derosa, Sahebkar, & Maffioli, 2018; Grygiel-Górniak, 2014). A well-known synthetic model agonist for the human PPARa is pirinixic acid (also known as 4-chloro-6[(2.3-dimethylphenyl)amino]-2-pyrimidinyl]thio-acetic acid or WY-14643) (Figure 1.1). WY-14643 has been used as an anti-hypercholesterolemic agent in humans where it promotes peroxisome proliferation. It is also used as an agonist in functional studies of PPARa (J. Z. Zhang & Ward, 2010; W. Zhang, Sakai, Fujiwara, & Hatano, 2017). PPARd is also activated by unsaturated fatty acids, carbaprostacyclin, and the synthetic aromatic ether, GW501516 (Billin, 2008). For PPARg no highly specific endogenous ligand is known, but it can be activated by prostaglandins and eicosanoids. Of exogenous and synthetic PPARg ligands there are several, including rosiglitazone, pioglitazone, troglitazone and ciglitazone, which are drugs that can be used in treatment of diabetes and cardiovascular diseases (Grygiel-Górniak, 2014; Guan, Ishizuka, Chui, Lehrke, & Lazar, 2005; Shang et al., 2018).

The PFASs share structural similarities to fatty acids (FA), which also have a hydrophobic carbon backbone of variable length with a hydrophilic carboxylate group at the end. In Figure 1.1 the structure of WY-14643, the three PFASs used in this study, as well as a saturated fatty acid (nonanoic acid) are shown. Accordingly, it has been found that hPPARa can be activated by PFOA, PFOS, propanoic acid (PMPP), ammonium perfluoro(2-methyl-3-oxahexanoate) (PMOH), perfluorohexanoic acid (PFHxA), perfluorohexanesulfonic acid (PFHxS), and perfluorobutanoic acid (PFBA). Furthermore, perfluorinated carboxylic acids have been shown to be agonists with higher efficacy than perflurorinated sulfonic acids (Behr, Plinsch, Braeuning, & Buhrke, 2020). There are also species differences regarding PPARs and activation by PFAS molecules. Studies conducted with mouse and human PPARa have

demonstrated that the receptors can be significantly activated by several PFASs, including PFOA, and PFOA was found to activate the mouse PPARd as well. PFOS was shown to activate the mouse PPARa, but not the human PPARa. Taken together, this demonstrates that PPARs are potential targets for PFASs, which therefore may modulate their activities, including the regulation of their target genes (Schlezinger et al., 2020; Takacs & Abbott, 2007).

1.2.2 Functional Domains of PPARs

PPARs have a canonical domain structure similar to other NRs, including five functional domains: A/B, C, D, E, and F (Fig. 1.3). The N-terminal A/B domain has a ligand-independent activation function (AF-1), which is responsible for receptor activation through phosphorylation (Werman et al., 1997). This is followed by the DNA-binding domain (DBD) in the C region, possessing two zinc fingers required for binding to peroxisome proliferator response elements (PPREs) in the promotor region of their target genes. The D domain includes a dimerization interface, which can dimerize to e.g. RXR to make a heterodimer. Situated between the DBD and LBD, the hinge (D region) provides flexibility in the PPAR receptors (Germain, Staels, Dacquet, Spedding, & Laudet, 2006; Kota, Huang, & Roufogalis, 2005). The E-region is the ligand-binding domain (LBD), responsible for specific recognizing, binding of ligands and activating the receptor (Kota et al., 2005). The ligand-dependent activation function (AF-2) is located in the F domain, which aid the recruitment of co-factors to assist the gene transcription of target genes (Kota et al., 2005; Tyagi et al., 2011; Zoete et al., 2007).

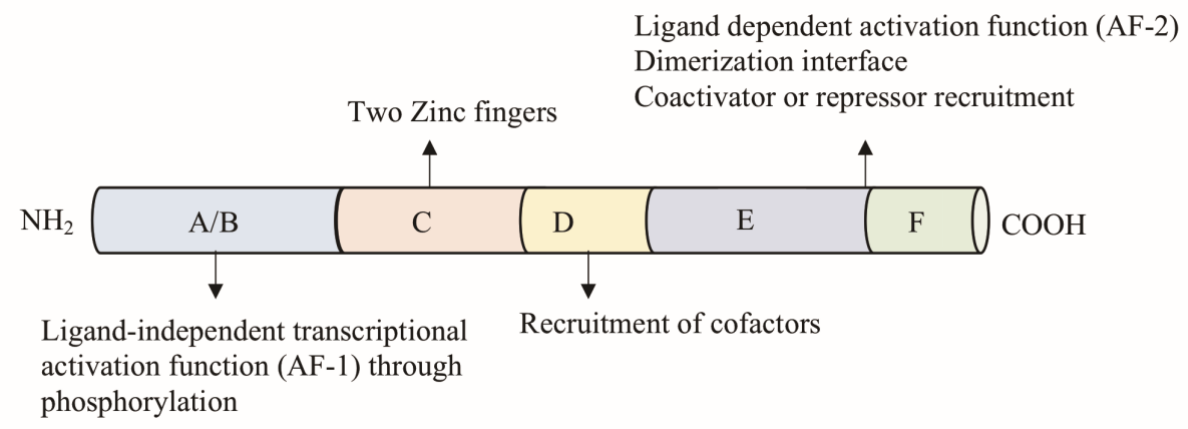

Figure 1.3: Functional domains of peroxisome proliferator-activated receptors. A linear representation of the functional domains of the peroxisome proliferator-activated receptor.

1.2.3 Mechanism of ligand activation of PPAR

Unliganded PPAR is located in the nucleus. When PPAR is activated by endogenous or exogenous ligands it heterodimerizes with 9-cis-retinoic X receptor (RXR), forming the heterodimer PPAR:RXR (Fig. 1.4). The binding of ligands also facilitates the release of co-repressors associated with PPAR, and the recruitment of cellular co-activators. The PPAR:RXR heterodimer will bind to PPREs in DNA allowing the initiation of the transcription of target genes (Kliewer, Umesono, Noonan, Heyman, & Evans, 1992). The function of PPAR is controlled at multiple levels, including ligand availability, protein-protein interactions, receptor abundance and stability, as well as posttranslational modifications (Kota et al., 2005; Patel, Truant, Rachubinski, & Capone, 2005).

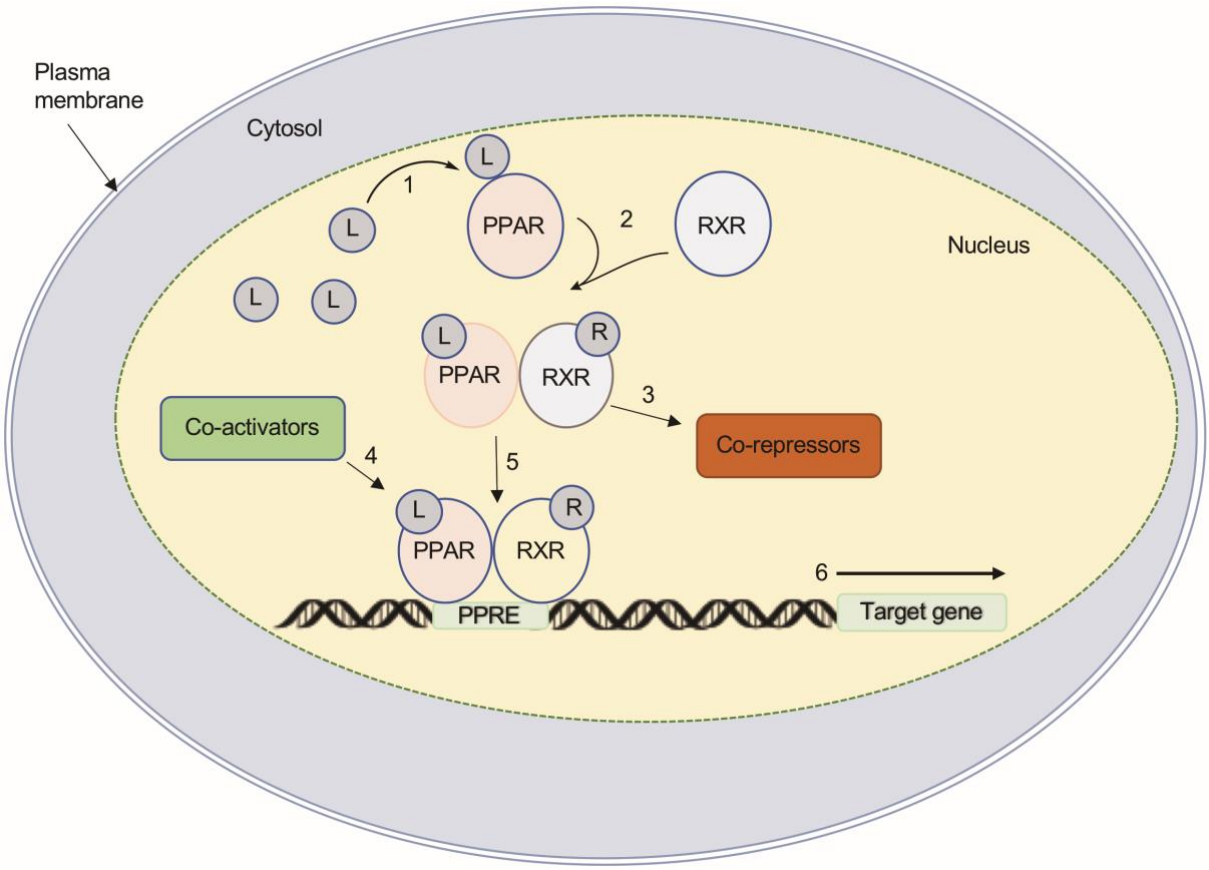

Figure 1.4: Mechanism of ligand activation of the peroxisome proliferator-activated receptor (PPAR). Unliganded PPAR is located to the nucleus. When PPAR recognizes and bind to a ligand (L) (1), the receptor will heterodimerize with retinoid X receptor (RXR) (R=intracellular RXR ligand) to form the heterodimer (PPAR:RXR) (2). The binding of ligand also facilitates release of co-repressors (3) and recruitment of co-activators (4). The PPAR:RXR heterodimer together with the co-activators binds to peroxisome proliferator response elements (PPREs) in the DNA (5) facilitating transcription of various PPAR target genes (6).

1.2.4 PPARs IN ATLANTIC COD

Four different Ppar-encoding genes have been identified in Atlantic cod, i.e. *gmppara1*, *gmppara2*, *gmppard*, and *gmpparg* (Eide et al., 2018; Sofie Söderstrøm, 2020), but their exact function is not known. However, the Atlantic cod Ppars were recently cloned and studied with regard to their phylogeny, ligand-activation, and tissue specific distribution (Sofie Söderstrøm, 2020). Earlier, PFOA and PFNA, but not PFOS, were shown to activate gmPpara1 in Atlantic cod, indicating that these compounds may act as endocrine disruptors by being able to modulate the energy metabolism (S.Söderstrøm, 2017). Notably, it was also demonstrated that gmPpara2 is not responsive to activation by PFASs (S.Söderstrøm, 2017). Comparison of the gmPpara1 and gmPpara2 primary structures demonstrated that gmPpara2 have an additional stretch of 14 amino acids (AAs) in its hinge region that is not present in gmPpara1 or hPPARa (Fig. 1.5). *In silico* modeling of the gmPpara1 and gmPpara2 3D structures suggested that this extended stretch of AAs forms an extended loop in the region between H1 and H3 in the gmPpara2 receptor (Fig. 1.6). This extended loop may introduce instability to the receptor structure that may have an impact on the function of gmPpara2. It has been demonstrated that the model-agonist WY-14643 binds in the canonical binding pocket of hPPARa. WY-14643 interacts with hPPARa by a hydrogen-bond network with the carboxylic functional group in the upper part of the site, and hydrophobic interactions with the site further down within its hydrophobic tail. It has also been confirmed that WY-14643 molecules can bind to a second allosteric site present in the ligand-binding pocket of the hPPARa receptor. This secondary binding site is positioned between helices 2 and 3 of the protein (H2 and H3), and it has been proposed that binding of WY-14643 to this second binding site stabilizes the structure of this region of the protein, which has been shown to be very flexible (Bernardes et al., 2013).

Importantly, the AAs involved in binding of WY-14643 in the primary binding site in the ligand-binding pocket of hPPARa are conserved in both gmPpara1 and gmPpara2, which correspond to S280, Y314, H440, and Y464 in hPPARa (Fig. 1.5). Accordingly, both gmPpara subtypes were activated by WY-14643, but gmPpara1 was the most sensitive receptor and produced the highest efficacy (S.Söderstrøm, 2017). The four AA residues constituting the putative second binding site for WY-14643 are also conserved in gmPpara1, with the exception of the conservative substitution of K278->R278 (Fig. 1.5). On the other hand, this site appears to be disrupted in gmPpara2, where two of these residues are substituted with AAs possessing other chemical properties, i.e. K278->G278 and H286->L286. These discrepancies, including

both the additional stretch of 14 (AAs) in the hinge region and the differences in the putative second binding site, may have an impact on the observed differences in both efficacy and potency of WY-14643 towards, and the activation by PFAS molecules in gmPpara1 compared to gmPpara2 (S.Söderstrøm, 2017).

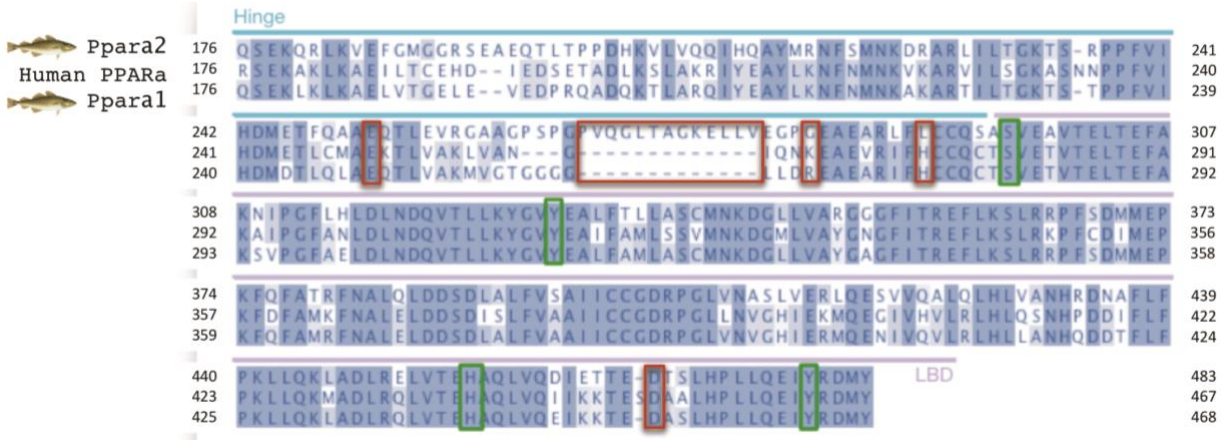

Figure 1.5: Multiple sequence alignment of human PPARa, Atlantic cod Ppara1 and Ppara2. The areas highlighted with red squares show the extended stretch of AA in the hinge region of gmPpara2, as well as the AAs that have been identified to constitute the second binding site for WY-14643 in hPPARa. The residues highlighted in green are conserved AAs important for binding of WY-14643 in the canonical binding site. This figure was modified from (S.Söderstrøm, 2017).

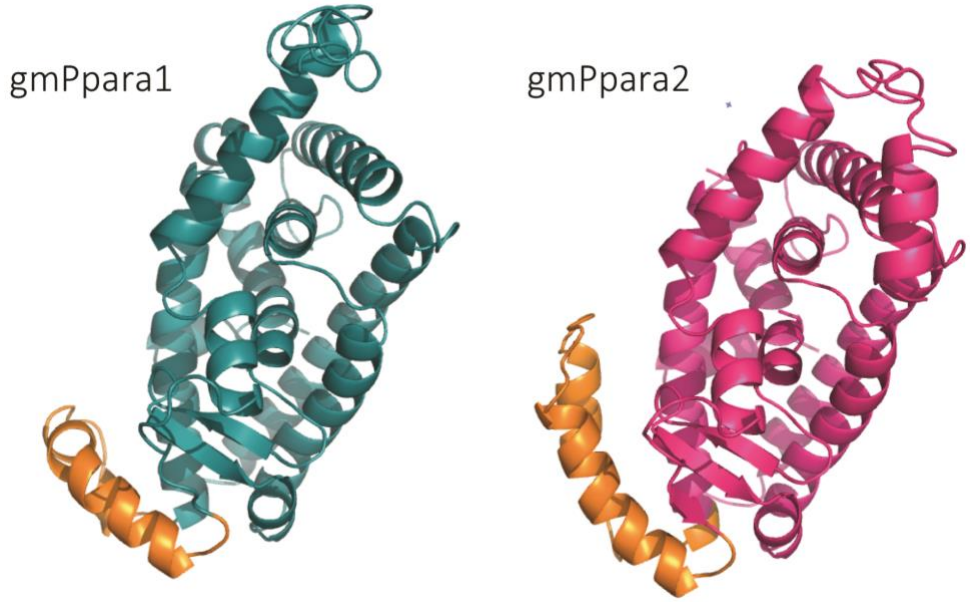

Figure 1.6: 3D-model of the hinge-region and ligand-binding domain of gmPpara1 and gmPpara2. The LBDs of the two receptors share structural features to other NRs. The hinge region between H1 and H3, which contain the additional stretch of 14 AA in gmPpara2 is shown in orange, and is, thought to produce an extended loop in comparison to gmPpara1. This extension is situated near both the LBP and the coregulator binding groove (AF-2 motif). The figure was made by collaborator Prof. Roland Stote, University of Strasbourg, France.

1.3 Atlantic cod as a model species

Atlantic cod (*Gadus morhua*) is a teleost that is abundant in the North Atlantic Ocean and the Barents Sea, with several populations differing in geographic distribution, life history strategy, and genetics. The north east Atlantic cod is the largest cod population in the world, which is also commercially highly important for Norwegian fisheries (Link, Bogstad, Sparholt, & Lilly, 2009).

The annotation of the Atlantic cod genome facilitates the ability to combine proteomics, genomics and metabolomics to investigate how cod respond to different environmental pollutants on several biological levels (Karlsen et al., 2011; Link et al., 2009; Star et al., 2011). Due to the position of Atlantic cod in the marine food chains it has a key role in coastal and pelagic ecosystems, and is often used as an indicator species in pollution monitoring programs (Link et al., 2009). Different environmental contaminants have been found to accumulate in cod and affect biomarker responses (Dale et al., 2019; Ono et al., 2019; Yadetie et al., 2016).

For instance, PCBs which is now forbidden to use, bioaccumulate and biomagnify in the food chain, and *in vivo* studies have revealed that this compound may affect the lipid metabolism cytoskeletal remodeling, cell cycle and cell adhesion in Atlantic cod (Yadetie et al., 2017).

1.4 AIM OF STUDY

Previous findings have shown that the Atlantic cod gmPpara1 and gmPpara2 have distinct differences in their primary structures (S.Söderstrøm, 2017). Among the major difference between the cod Ppara1 and Ppara2 is a 14 AA indel in the hinge region (AA 266-279), putatively producing an extended loop between H1 and H3 in the gmPpara2 protein structure that could possibly destabilize this region (Fig. 1.6). Structural analyses *in silico* suggested that this indel could contribute to the observed discrepancies in the activation profiles produced in luciferase-based reporter gene system when exposed to various ligands, including both PFASs and the WY-14643 model agonist. Furthermore, the AAs shown to constitute a second binding site for the WY14643 model-agonist in the hPPARa are different in the gmPpara protein sequences, although this second binding site has not yet been confirmed to bind WY-14643 in the gmPpars. In gmPpara1, two of the AAs that are part of this site are arginine (R278) and a histidine (H286), which both are reactive AAs. In gmPpara2 these AAs have been substituted to the more aliphatic and non-reactive glycine (G278) and leucine (L286). Moreover, we hypothesize that the extended AA stretch in hinge region of gmPpara2, in addition to the differences in AA in the putative second binding site for WY-14643, can affect the transactivation of gmPpara2 *in vitro*. Thus, in order to assess these differences, the stretch of 14 AA in gmPpara2 will be deleted, and in addition the AAs constituting the putative second WY14643-binding will be mutated to become similar to gmPpara1. To functionally characterize the receptors, the transactivation profiles of the wild type and mutated gmPpara proteins will be analyzed in a luciferase-based reporter gene assay with the model-agonist WY-14643 and three PFASs, including PFOA, PFNA and PFOS, where PFOA and PFNA were previously shown to activate gmPpara1, but not gmPpara2. We hypothesize that when gmPpara2 become gradually more similar to gmPpara1, it will also be activated by PFOA and PFNA.

2. MATERIALS

2.1 CHEMICALS AND REAGENT

Table 2.1: Chemicals and reagents used during the master thesis.

Name	CAS #	Supplier
10x Loading Buffer		TaKaRA
2-log DNA ladder	N3200s	New England Biolabs
5-CFDA-AM (5-Carboxyfluorescein Diacetate, Acetoxymethyl Ester)	124412-00-6	Thermo Fisher Scientific
Agar	9002-18-0	Merck
Agarose	9012-36-6	Sigma-Aldrich
Ampicillin sodium salt	69-52-3	Sigma-Aldrich
(Adenosine 5´-triphosphate disodium salt(ATP)	34369-07-8	Sigma-Aldrich
β-mercaptoethanol	60-24-2	Sigma-Aldrich
Bovine Serum Albumin (BSA)	9048-46-8	Sigma-Aldrich
3-((3-cholamidopropyl) dimethylammonio)-1-propanesulfonate (CHAPS)	75621-03-3	Appli Chem
Charcoal stripped Fetal bovine serum		Biowest
Coenzyme – A	18439-24-2	Fisher Scientific
Disodium hydrogen phosphate	30435	Sigma-Aldrich
D-luciferin potassium salt	115144-35-9	Biosynth
Dimethyl sulfoxide (DMSO)	67-68-5	Sigma-Aldrich
Dulbecco's Modified Eagle's Medium (high glucose, with phenol red)	D5671	Sigma-Aldrich
Dulbecco's Modified Eagle's Medium (high glucose, without phenol red)	D1145	Sigma-Aldrich
(Ethylenediaminetetraacetic acid disodium salt dehydrate) EDTA	6381-92-6	Sigma-Aldrich
(Ethylene glycol-bis(2-aminoethylether)-N,N,N´,N´-tetraacetic acid) EGTA	67-42-5	Sigma-Aldrich
Ethanol	64-17-5	Sigma-Aldrich
Fetal bovine serum (FBS)	F7524	Sigma-Aldrich
Gel-Red	41003	Biotium
Glycerol	56-81-5	Sigma-Aldrich
L-glutamine	56-85-9	Sigma-Aldrich
L-α-Phosphatidylcholine	8002-43-5	Sigma-Aldrich
Magnesium carbonate hydroxide pentahydrate -	56378-72-4	Sigma-Aldrich
Magnesium chloride hexahydrate -	7791-18-6	Sigma-Aldrich
Magnesium sulfate heptahydrate	10034-99-8	Sigma-Aldrich
Methanol	67-56-1	Sigma-Aldrich
ONPG (2-Nitrophenyl β-D-galactopyranoside)	369-07-3	Sigma Aldrich
Opti-MEM ® (1X)	31985062	Gibco

PFNA (Perfluorononanoic acid)	375-95-1	Sigma Aldrich
PFOA (Perfluorooctanoic acid)	335-67-1	Sigma Aldrich
PFOS (Perfluorooctanesulfonic acid)	1763-23-1	Sigma Aldrich
Penicillin streptomycin	P4458	Sigma Aldrich
Phosphate-buffered saline (PBS) 10X	P5493	Sigma Aldrich
PMSF (Phenylmetanesulfonyl fluoride)	329-98-6	Sigma Aldrich
Potassium Chloride	7447-40-7	Sigma Aldrich
Precision Plus Protein™ Kaleidoscope™	1610373	Bio-Rad
Resazurin sodium salt	62758-13-8	Sigma Aldrich
SOC Outgrotwth Medium	B9020S	New England Biolabs
Sodium Chloride	7647-14-5	Merck Millipore
Sodium phosphate monobasic monohydrate	10049-21-5	Merck Millipore
Sodium pyruvate solution	113-246	Sigma Aldrich
TransIT ®-LT1	MIR2300	Mirus Bio LLC
Tricine	5704-04-1	Sigma Aldrich
Tris-HCl pH 7.8	T2913	Sigma Aldrich
Triton® X100	9002-93-1	Sigma Aldrich
Tryptone plus	91079-40-2	Sigma Aldrich
Yeast Extract	Y1625	Sigma Aldrich
WY-14643	50892-23-4	Sigma Aldrich

2.2 SOFTWARE

Table 2.2: Software and online tools used during the thesis.

Software	Application	Provider
ChemDraw	Figures	PerkinElmer
Clustal Omega	Sequence Alignments	EMBL-BI
EnSpire Manager	Operate plate reader	PerkinElmer
Excel 2020 (version 16.35)	Data analysis and statistics	Microsoft
ExPASy Translate tool	Sequence translation	SIB Bioinformatics Resource Portal
ExPASy Compute pI/Mw tool	Computation of theoretical Mw	SIB Bioinformatics Resource Portal
Jalview 2.11.1.0	Alignments	Waterhouse, Procter, Martin, Clamp, and Barton (2009)
GraphPad Prism 8	Figures and statistics	GraphPad Software
NEBase Changer	Primer Design	New England Biolabs
NanoDrop Software	Spectrophotometry	Thermo Fisher Scientific
PowerPoint 2020 (version 16.35)	Figures	Microsoft®
QuikChange® Primer Design Program	Primer Design	Agilent Technologies

2.3 EQUIPMENT AND INSTRUMENTS

Table 2.3: Equipment and instruments utilized during the thesis.

Instrument	Application	Supplier
Bürker haemocytometer	Cell counting	Marienfield
ChemiDoc™ XRS+ System	Gel scanning	Bio-Rad
Doppio Thermal Cycler	PCR Thermo Cycler	VWR
EnSpire 2300 Multimode Reader	Plate reader	PerkinElmer
HS 501 Digital	Platform shaker	IKA-Werke
NanoDrop 1000	Spectrophotometer	Thermo Scientific
PowerPac™ HC	High-current power supply	Bio-Rad
Thermomixer compact	Heat block	Eppendorf
Ultraspec 10 Cell density meter	Culture density	Amersham Biosciences
Z 216 MK microliter centrifuge	Centrifuge	Hermle

2.4 PRIMERS

Table 2.4: Primers used for creating mutants of gmPpara2

Name	Usage	Sequence 5'→3'
DEL Fwd	NEB Q5	5'-GGGCCCGGCGAGGCAGAG
DEL Rev	NEB Q5	5'-GCCGGGGCTAGGCCCTGC
t299a Fwd	Agilent QuikChange	5'-CTCTGGCAGCAG**T**GGAACAGCCGGG
t299a Rev	Agilent QuikChange	5'-CCCGGCTGTTCC**A**CTGCTGCCAG
g274c g275g c276c FWD	Agilent QuikChange	5'-CCCCGGCGGGCCC**CGC**GAG GCAGAGGCCC
g274c g275g c276c REV	Agilent QuikChange	5'-GGGCCTCTGCCTC**GCG**GGG CCCGCCGGGG

2.5 PLASMIDS

Table 2.5: Plasmid concentrations and purities used for LRA, cytotoxicity measurements and SDS-PAGE.

Plasmid	Concentration [ng/µL]	$A_{260/280}$	$A_{260/230}$
pCMV_β-galactosidase	1523	1.89	2.30
(MH100)x4tk luciferase	1724	1.89	2.34
pCMX_GAL4_gmPpara1	2734	1.91	2.37
pCMX_GAL4_gmPpara2	1640	1.90	2.40
pCMX-GAL4_gmPpara2_DEL	1793	1.91	2.40
pCMX-GAL4_gmPpara2_DEL_G>R	1922	1.91	2.39
pCMX-GAL4_gmPpara2_DEL_L>H	1807	1.89	2.40
pCMX-GAL4_gmPpara2_DEL_G>R+L>H	2426	1.89	2.37

2.6 COMMERCIAL KITS

Table 2.6: Commercial kits utilized during the thesis.

Name	Usage	Supplier
Q5® Site-Directed Mutagenesis kit	Constructing mutants	New England Biolabs
QuikChange II Site-Directed Mutagenesis kit	Constructing mutants	Agilent Technologies
NucleoBond® Xtra Midi plasmid purification kit	Plasmid purification	Macherey-Nagel
NucleoSpin® Plasmid EasyPure kit	Plasmid purification	Macherey-Nagel
SuperSignal West Pico Chemiluminescent Substrate	Protein detection (Western blotting)	Thermo Scientific
	Protein detection (Western blotting)	Thermo Scientific

2.7 BACTERIA AND CELL LINES

Table 2.7: Bacteria and cell lines utilized during the thesis.

Cell line	Application	Supplier/reference
COS-7 cells	Eukaryote expression	(Gluzman, 1981)
StrataClone Solo Pack Competent Cells	Prokaryote cloning	Agilent

2.8 GROWTH MEDIA

Table 2.8: Lysogeny Broth (LB) growth media

Component	LB-Agar (plates)	LB-Media
Tryptone	10 g/L	10 g/L
Yeast extract	5 g/L	5 g/L
Sodium chloride	10 g/L	10 g/L
Agar-agar	15 g/L	-
[i]Ampicillin	100 mg/L	100 mg/L
Deionized H_2O	-	-

[i]Added after autoclaving for 30 min at 121^{o}C.

Table 2.9: Cell Freezing media for COS-7 cells

Component	Conc.
Dulbecco's modified Eagle medium (DMEM) with phenol red	1X
Fetal bovine serum (FBS)	10 %
L-glutamine	4 mM
Sodium pyruvate	1 mM
Penicillin-Streptomycin	100 U/mL
Dimethyl sulfoxide (DMSO)	5 % (v/v)

Table 2.10: Growth media for cultivation of COS-7 cells

Component	Conc.
Dulbecco's modified Eagle medium (DMEM)[i]	1X
Fetal bovine serum (FBS)[ii]	10 %
L-glutamine	4 mM
Sodium-pyruvate	1 mM
Penicillin-Streptomycin	100 U/mL

[i]Cell growth media was made with DMEM with phenol red, while phenol red-free DMEM was used in exposure media.

[ii]Charcoal-stripped FBS was used in exposure media.

2.9 BUFFERS AND SOLUTIONS

2.9.1 AGAROSE SOLUTIONS

Table 2.11: Tris borate EDTA (TBE) buffer

Component	Conc.
Tris	0.45 M
Boric acid	0.45 M
EDTA	0.01 M
Deionized-H_2O	-

Table 2.12: Agarose gel components

Component	Conc.
TBE- buffer (Table 2.11)	0.5 X
Agarose	0.7 %
GelRed	0.0002 %

Table 2.13: Agarose gel components

Component	Conc.
TBE- buffer (Table 2.x)	0.5 X
Agarose	0.7 %
GelRed	0.0002 %

2.9.2 LUCIFERASE REPORTER GENE ASSAY (LRA)

Table 2.14: Cell lysis base buffer (1X)

Component	Conc.
Tris-HCl (pH 7.8)	25 mM
Glycerol	15 %
CHAPS	2 %
L-α-Phosphatidylcholine	1 %
BSA	1 %

Table 2.15: Cell lysis reagent solution

Component	Conc.
Lysis base buffer (Table 2.x)	1 X
EGTA	4 mM
$MgCl_2$	8 mM
PMSF	0.4 mM
DTT	1 mM

Table 2.16: β-galactosidase base buffer (10 X)

Component	Conc.
Na_2HPO_4	60 mM
NaH_2PO_4	40 mM
KCl	10 mM
$MgCl_2$	1 mM

Table 2.17: β-galactosidase reaction solution

Component	Conc.
β-galactosidase buffer 1X (Table 2.16)	1 X
β-mercaptoethanol	52.9 mM
ONPG	8.6 mM

Table 2.18: Luciferase base buffer (4X, pH 7.8)

Component	Conc.
Tricine	80 mM
$(MgCO_3)_4$-$Mg(OH)_2$*$5H_2O$	4.28 mM
Na_2EDTA	0.4 mM
$MgSO_4$*$7H_2O$	10.68 mM

Table 2.19: Luciferase reaction solution

Component	Conc.
Luciferase base buffer (Table 2.18)	1 X
ATP	0.5 mM
DTT	5 mM
Coenzyme A[i]	0.2 mM
D-luciferin[i]	0.5 mM

[i]Added just before use

2.9.3 CELL VIABILITY

Table 2.20: L-15/ex Solution A

Component	Conc.
NaCl	80 g
KCl	4 g
$MgSO_4$-7*H_2O	2 g
$MgCl_2$-6*H_2O	2 g
Deionized-H_2O	600 mL

Table 2.21: L-15/ex Solution B

Component	Conc.
1.4 g $CaCl_2$	1.4 g
Deionized-H_2O	100 mL

Table 2.22: L-15/ex Solution C

Component	Conc.
Na_2HPO_4	1.9 g
KH_2PO_4	0.6 g
Deionized-H_2O	300 mL

Table 2.23: L-15/ex solution for cell viability measurements

Component	Conc.
Solution A (Table 20)	34 mL
Solution B (Table 21)	6 mL
Solution C (Table 22)	17 mL
Galactose 90	0.8 mg/mL
Pyruvate	0.5 mg/mL
Di-H_2O	500 mL

Table 2.24: Viability solution with resazurin and CFDA-AM

Component	Conc.
L-15/ex	1 X
Resazurin	0.03 mg/mL
CFDA-AM	0.001 mM

2.9.4 SDS-PAGE

Table 2.25: 5X SDS-PAGE Sample Buffer (5XSB)

Component	Conc.
TrisHCl pH 6.8	250 mM
SDS	10 %
Glycerol	30 %
β-mercaptoethanol	5 %
Bromophenolblue	0.02 %

Table 2.26: Lysis Reagent for preparation of proteins for SDS-PAGE

Component	Conc.
5X sample buffer	2.0 X
10 X PBS pH 7.4	1.0 X
Protease inhibitor (P8340)	1.0 X
Deionized-H_2O	-

Table 2.27: SDS-PAGE 10 % Resolving Gel and 4 % Stacking Gel

Component	Conc.	Conc.
Tris-HCl (pH 8.8)	375 mM	-
Tris-HCl (pH 6.8)	-	125 mM
Acrylamide/bisacrylamide	10 %	4 %
Sodium dodecylsulfate (SDS)	0.1 %	0.1 %
Ammonium persulfate (APS)	0.1 %	0.1 %
N, N, N', N', Tetramethylethane-1.2-diamine (TEMED)	0.1 %	0.2 %

Table 2.28: 1 X SDS-PAGE running buffer

Component	Conc.
Trisma base	25 mM
Glycine	192 mM
SDS	0.1 %

Table 2.29: 1 X Blotting Buffer

Component	Conc.
Tris	25 mM
Glycine	192 mM
Methanol	20 %
Deionized-H_2O	-

Table 2.30: 5X Tris Buffer Saline (TBS) (pH 7.5)

Component	Conc.
Tris	24 g
NaCl	292.5 g
Deionized -H_2O	2000 mL

Table 2.31: Protein immunoblotting washing solution 0.05 % TBS-Tween

Component	Conc.
5 X TBS (Table 2.x)	1 X
Tween 20	0.05 %
Deionized-H_2O	-

Table 2.32: Blocking solution with 5 % Dry Milk

Component	Conc.
Dry milk	6.25 g
TBS-Tween (Table 2.31)	125 mL

Table 2.33: Antibodies used for western blotting during the thesis.

Name	Supplier
GAL4 (DBD) (RK5C1), mouse monoclonal	Santa Cruz Biotechnology
Anti-β-actin, monoclonal	Abcam
Horseradish Peroxidase linked whole antibody from sheep Anti-mouse IgG, polyclonal	GE Healthcare UK Limited

3. METHODS

3.1 EXPERIMENTAL OUTLINE

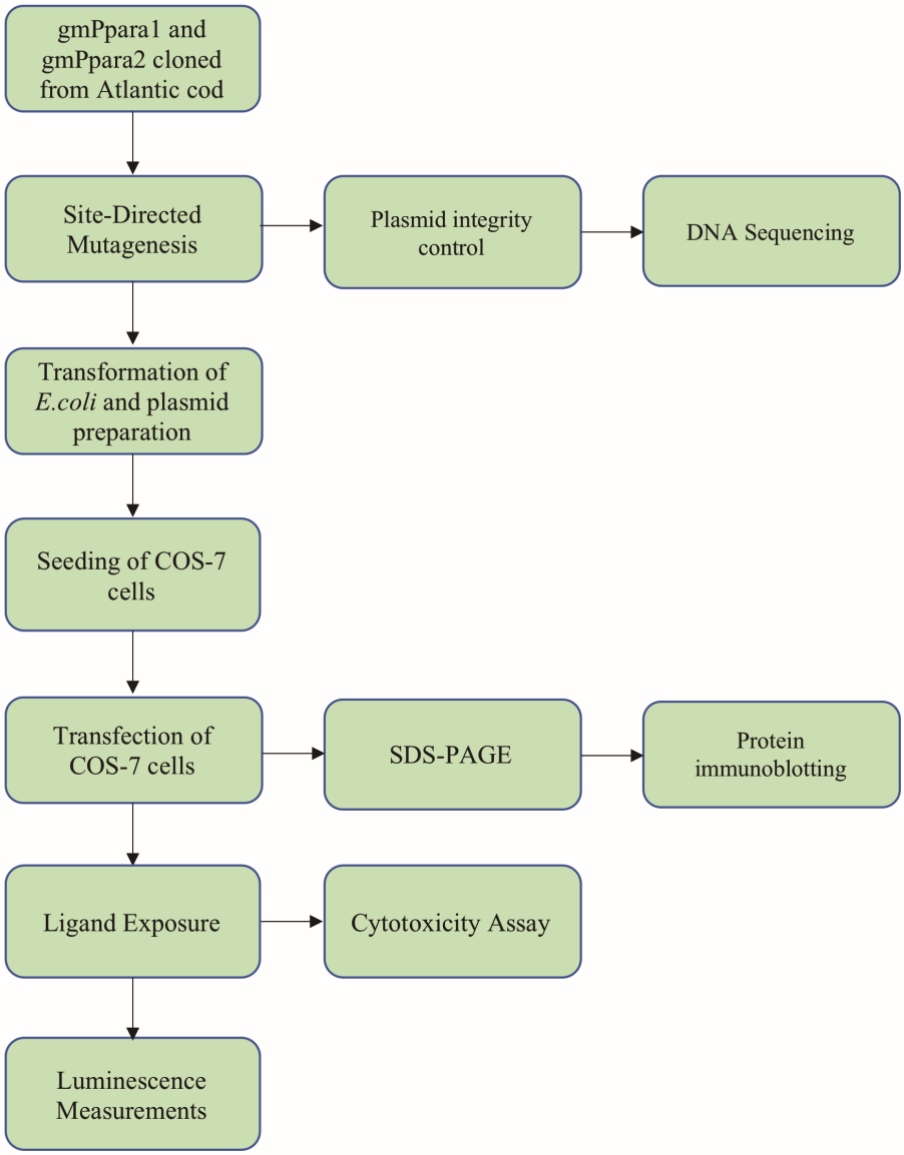

Figure 3.1: Workflow overview. Site-directed mutagenesis was used to generate four different gmPpara2 mutants, which were verified with Sanger sequencing. Highly pure plasmids (Table 2.5) were prepared with midi-preparations for the luciferase reporter gene assay (LRA), and the integrity of plasmids was assessed by agarose gel electrophoresis prior to use. In the luciferase reporter gene assay, COS-7 cells were seeded and transiently transfected with plasmids encoding wt and mutated gmPparas, as well as reporter and control plasmids. The transfected COS-7 cells were exposed to selected ligands (WY-14643, PFOA, PFNA and PFOS), and luciferase activity was recorded the next day. To assess the expression of gmPpar-fusion proteins in the COS-7 cells, the transfected cells were harvested, proteins separated by SDS-PAGE and fusion proteins detected by protein immunoblotting. The cytotoxicity of the test compounds, were evaluated by measuring effects on metabolic activity and membrane integrity.

3.2 Construction of Atlantic cod Ppara2 mutant plasmids

3.2.1 Preparation of plasmids encoding mutated gmPpars

Eukaryotic expression plasmids encoding the Atlantic cod Ppara1 and Ppara2 (pCMX-GAL4_gmPpara1/2) (previously prepared by Sofie Söderstrøm Oct. 2017), were used as templates for construction of plasmids encoding mutated gmPpars. In these pCMX-GAL4_gmPparx plasmids, the hinge region and the LBD of the gmPparx receptor is fused N-terminally to the DBD of yeast GAL4, encoding GAL4-DBD-gmPparx-LBD fusion protein.

3.2.2 Site directed mutagenesis

Site directed mutagenesis (SDM) is an *in vitro* technique that allows for changing single or multiple nucleotides, as well as removing or inserting nucleotides in a DNA sequence to alter the encoded AA sequence, or change the reading frame (Agilent). In this study two different mutagenesis kits was used to perform two different types of mutations. The NEBQ5 kit was used to delete a stretch of 14 AAs (AA 266 to 279) in gmPpara2, while the Agilent QuikChange kit was used for making two point mutations in gmPpara2, i.e. to change G278>R278 and L286>H286.

3.2.2.1 Deletion of 14 AAs in gmPpara2

Primers were designed using the online tool of NEBQ5 NEBase Changer (https://nebasechanger.neb.com, April 2020). The primers used are shown in Table 2.3. Deletions to pCMX-GAL4_gmPpara2 were performed using the NEBQ5 SDM kit reaction solutions as described in Table 3.1, and a temperature cycle as described in Table 3.2. Prior to circularization of the linear PCR product.

The linear amplification products were ligated with NEB Q5 SDMs KLD enzyme mix, which contains a kinase to phosphorylate the 5'-end of the PCR-product, a ligase to ligate the two ends of the linear PCR product together, and DpnI, which cleaves template DNA containing methylated adenine ($_m$A) at the dam sequence G$_m$A | TC. The ligation was performed at RT for five minutes.

Table 3.1: Reaction solution for NEB Q5 SDM deletion experiment

Reagent	25 µL RXN	Conc.
Q5 Hot Start High-Fidelity 2X Master Mix	12.5 µL	1 X
10 µM Fwd Primer	1.25 µL	0.5 µM
10 µM Rev Primer	1.25 µL	0.5 µM
Plasmid	10 ng	
DI-H_2O	25-x L	

Table 3.2: Thermal cycle program for NEB Q5 SDM deletion experiment

Step	Temp. (^oC)	Time
Initial Denaturation	98	30 sec
25 cycles	98	10 sec
	76	30 sec
	72	3 min
Final Extension	72	2 min
Hold	4	

Transformation and selective cultivation of transformed E.coli

To transfer the circular mutated DNA to bacteria, NEB alpha *E. coli* competent cells were transformed by heat shock treatment. The transformation mixture was prepared with 5 µL of ligation mixture and 25 µL of competent *E. coli* cells. The cells were kept on ice for 30 min to ensure an abrupt temperature change. The heat shock was performed in a 42 ^oC water bath for 30 sec, immediately incubating the cells on ice for five minutes. To cultivate the transformed cells, 950 µl SOC medium was added to each reaction, and incubated at 37^oC for 1 hr while shaking. Subsequently, volumes of 10 µL and 100 µL of the transformation reaction were transferred to LB-agar plates (100 µg/mL amp), and incubated ON at 37^oC. Positive transformants were selected for by their ampicillin-resistance, provided by the Amp_r-gene in the cloning vector. Five colonies were selected and propagated in 3 mL LB-cultures, 100 µg/mL amp. The cultures were incubated ON at 37 ^oC, at 100 rpm shaking. These colonies were also reseeded on a new agar plate for further downstream use. The 3 mL cultures were used as templates to purify potentially mutated plasmids, and Sanger DNA sequencing (Method 3.8) was performed to evaluate the success of the SDM reactions. Plasmids from one clone encoding the desired deletion were chosen for further work. This mutant plasmid was named pCMX_GAL4_gmPpara2_DEL.

3.2.2.2 SINGLE AMINO ACID SUBSTITUTIONS IN GMPPARA2_DEL

To obtain the single AA changes in gmPpara2, point mutations were performed in the gmPpara2_DEL plasmid using the QuikChange II Site-Directed Mutagenesis kit. The primers

were designed using the online tool, the QuikChange® Primer Design Program (https://www.agilent.com/store/primerDesignProgram.jsp). Two AAs were targeted for substitution, G278 and L286. The goal was to produce two single AA (either R278 or H286) mutants and one double AA (both R278 and H286) mutant. Three reactions were prepared according to Table 3.3. The PCR was run as shown in Table 3.4.

Table 3.3: Reaction solution for Agilent QuikChange Mutagenesis.

Reagent	25 µL RXN	Conc.
10 X rxn buffer	2.5 µL	1 X
dsDNA template	3.45 µL	50 ng
Fwd primer	1.0 µL	125 ng
Rev primer	1.0 µL	125 ng
dNTP mix	0.5 µL	
dd H_2O	15.55 µL	

Table 3.4: Thermal Cycle program for QuikChange SDM point mutations.

Step	Temp. (°C)	Time
Initial Denaturation	95	30 sec
30 cycles	95	30 sec
	55	1 min
	68	6 min

DpnI digestion of template plasmid

To each reaction 1 µL DpnI restriction enzyme (10 U/ µL) were added, and incubated for 1 hr at 37°C, to digest parental plasmid DNA.

Transformation of competent E. coli cells and selective cultivation of transformed E.coli

The DpnI-digested SDM-products were transferred to StrataCloneSoloPack Competent Cells by heat shock transformation. The transformation mixtures were prepared by adding 1.5 µL of DpnI-digested SDM-product to 33 µL of competent cells. The transformation reactions were kept on ice for 30 min, then heat shocked at 42 °C in a water bath for 30 seconds, and immediately placed on ice for 5 minutes. To the heat shocked cells were added 250 µL SOC growth medium and incubated for 1 hr while shaking at 37°C. 25 µL and 200 µL reaction solution was plated on LB-Amp agar plates that were incubated ON at 37°C. 3 mL LB-Amp cultures were cultivated for plasmid preparation and purification (Methode 3.3.1). In total four different gmPpara2-mutants have been constructed (Table 2.5).

3.3 PLASMID DNA PURIFICATION

DNA purification was used to purify plasmids for later experiments. Small-scale plasmid preparation (mini-prep) (3.3.1) is a method suitable for purifying smaller amounts of DNA, e.g. plasmids for DNA sequencing. Medium-scale plasmid preparations (midi-prep) (3.3.2) is a method suitable for purifying larger amounts of highly pure plasmid DNA (pDNA), e.g. for the luciferase reporter gene assay LRA. The principle of the two methods are very similar, but midi-prep contains an additional concentrating and purifying step involving isopropanol precipitation (concentrating) and ethanol wash (desalting).

Transformed *E. coli* was inoculated in 3 or 200 mL LB-medium cultures containing 100 µg/mL ampicillin and cultivated overnight (37$_o$C, 250 rpm). The bacteria were harvested by centrifugation (3500xg, 5 minutes) and the pellet was resuspended in resuspension buffer containing RNase to degrade RNA. The DNA content of the *E. coli* host cells was liberated by SDS/alkaline lysis, followed by neutralization with a buffer containing acetate to make the plasmid DNA go back to its supercoiled conformation and ensure appropriate conditions for binding of plasmid DNA to the silica membrane. Chromosomal DNA, proteins and cell debris were precipitated by centrifugation, while the plasmid containing supernatant was applied to a silica-based column under high ionic conditions to bind pDNA. The membranes were washed with an ethanolic buffer to remove contaminations, such as macromolecular cellular components, salts, and metabolites. The pure plasmid DNA was eluted with an elution buffer with low ionic strength and slightly alkaline pH (Buffer AE, (5mM Tris/HCl, pH 8.5) for the mini-prep protocol. Midi-prep had an additional purification step where the DNA was precipitated with isopropanol and centrifuged, the pellet was washed with ethanol and dried. The pellet was dissolved in AE-buffer. The plasmid DNA concentrations were measured with Nanodrop.

3.3.1 SMALL-SCALE PLASMID PREPARATION

Small-scale plasmid preparations were performed to produce plasmids for evaluation of the SDM success by DNA sequencing. Selected *E. coli* transformants were inoculated ON. For purification of plasmid DNA, a NucleoSpin ® kit from Macherey-Nagel was used and the protocol followed. The plasmids were eluted with 50 µL AE buffer.

3.3.2 Medium-scale plasmid preparation

For purification of effector-, control-, and receptor plasmids used in the LRA (3.4), the Plasmid DNA purification NucleoBond® PC100 kit from Macherey-Nagel was used. *E. coli* was transformed with either the effector-, control- or receptor plasmid and inoculated separately. The density of the culture was measured at 600 nm using a cell density meter (Ultraspec 10 Cell Density meter, Amersham Biosciences). The ODV=200 was calculated (ODV=Optical density * culture volume (mL)). The plasmids were harvested, isolated, and purified according to the protocol. Purified plasmids were dissolved in 250 µL AE buffer.

3.4 Luciferase reporter gene assays (LRA) of gmPPARs

A COS-7 cell based UAS/GAL4-DBD luciferase reporter gene assay (LRA) was used to measure ligand activation of the gmPpars exposed to selected test compounds. A reporter plasmid (MH(100)x4tkluc) containing the luciferase reporter gene, a receptor plasmid (pCMX-GAL4_gmPparax), and a β-galactosidase-encoding control plasmid (pCMV_β_Gal) were transiently co-transfected into COS-7 cells. In the reporter plasmid the transcription of luciferase is controlled by repeated upstream activation sequences (GAL4-UAS) in the promotor region. The receptor plasmid encodes the fusion protein GAL4-DBD-gmPparx-hinge-LBD. Upon binding of an agonist to the LBD of the fusion protein, a conformation change occurs changing the GAL4_DBD_gmPparLBD fusion proteins from a non-active to an active state. This will assemble the transcription complex and initiate transcription of the luciferase-encoding gene. Luciferase will then be translated to protein, and the amount of luciferase produced can be determined by measuring the activity of the enzyme. When luciferase oxidizes the substrate luciferin to oxy-luciferin, light is emitted. This light can be measured at 560 nm and quantified, and correlated to the activation of the gmPparx receptor (Fig. 3.2). As β-galactosidase (β-gal) is continuously produced in the COS-7 cells, its activity can be used to normalize luciferase activities for variation in transfection efficacy between wells. β-gal hydrolyzes ONPG to ONP and galactose. ONP has a yellow color that absorbs light of 420 nm, and consequently the β-gal activity can be measured as absorbance.

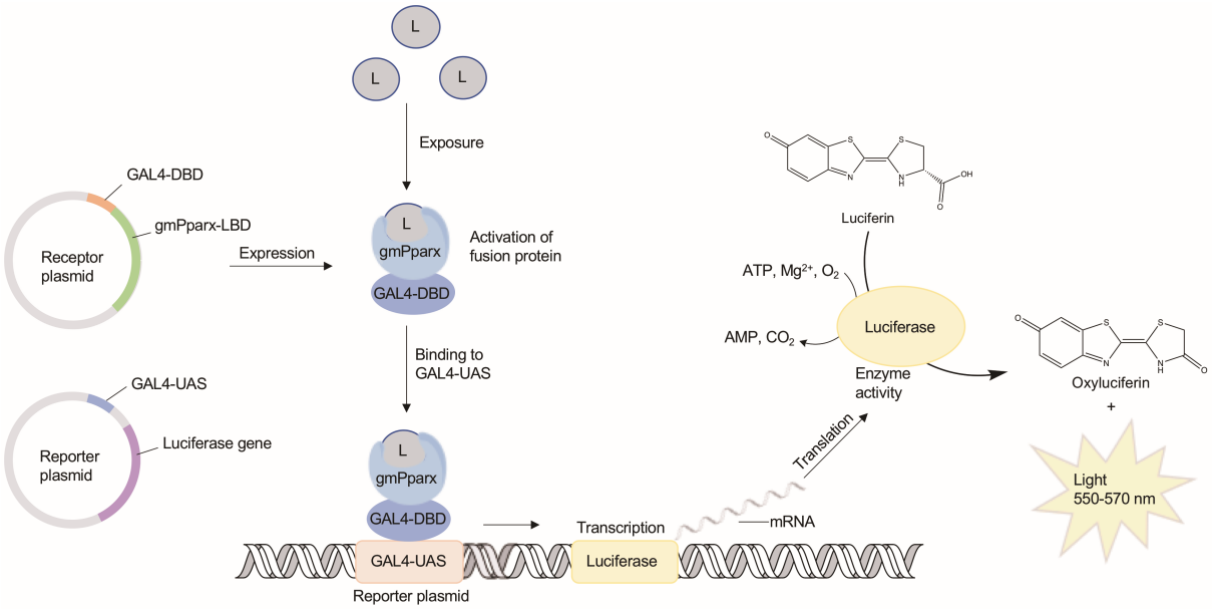

Figure 3.2: Overview of the principle behind the luciferase based GAL4-DBD UAS-system. COS-7 cells are co-transfected with a reporter plasmid encoding fusion proteins of GAL4_DBD and the hinge and LBD of gmPparax, together with the luciferase reporter gene plasmid and a β-galactosidase-encoding control plasmid (the latter not shown in the figure). When the fusion protein is activated by an agonist it binds to the GAL-4-upstream activation sequence (UAS) in the luciferase reporter plasmid. This facilitates transcription of the luciferase enzyme, which further oxidizes luciferin to oxy-luciferin and light. The light emitted at 550-570 nm can be quantified with a luminometer. The illustration is modified from Madsen (2016).

3.4.1 Control of LRA Plasmid Integrity

The effectiveness of transfection partly depends on plasmid quality. The integrity of the plasmids used in the LRA assay (receptor-, effector-, and control plasmids) was assessed with agarose gel electrophoresis (3.7) to ensure that the majority of the plasmids were in a supercoiled conformation, which is optimal for transfection into cells. The different conformations: circular nicked, linear and supercoiled were separated according to their migration distances in the gel, where supercoiled migrated the longest in the gel.

3.4.2 Cultivation of COS-7 Cells

COS-7 cells are an African green monkey kidney fibroblast-like cell line (Table 2.7). They grow in a monolayer in petri dishes, adhering to the surface. The cells were stored in freezing medium (Table 2.9) in liquid nitrogen. Aliquots were thawed at RT and resuspended in 10 mL COS-7 growth medium (Table 2.10), and centrifuged at 1000 x g at RT for 5 minutes. The

resuspension medium was removed, and 10 mL fresh medium was added to the cells (Table 2.10). The cells were seeded in 10 cm petri dishes and incubated at 37 ^{o}C, 5 % CO_2. The cultures were subcultured when they reached 90-100 % confluency. Old medium was removed, the cells washed with 1X PBS (pH 7.4), detached through trypsination with 0.05 % Trypsin-EDTA for 30 sec at RT, and incubated for 5 min at 37^{o}C, 5 % CO_2. Detached cells were resuspended in 10 mL fresh growth medium and usually diluted 1:10 or 1:20 for further culturing.

3.4.3 Seeding of COS-7 cells in 96-well plates

When COS-7 cells grown in culturing dishes reached 90-100 % confluency, the cells were washed, trypsinated and resuspended as described (3.4.2). Small equal volumes of cell suspension and of the dye, erythrosin-B, were mixed and cell density was determined using a Bürker hemocytometer (Marienfield) and a light microscope (Leica DM IL inverted microscope). COS-7 cells were seeded in 96-well plates using 100 µL growth medium with a final cell density of 5000 cells per well. The cells were incubated at 37 ^{o}C, 5 % CO_2 for 24 hr.

3.4.4 Transfection of COS-7 cells

Transient transfection introduces foreign DNA into a eukaryotic cell. The introduced DNA does not become part of the genome of the cell, and hence the plasmids will be expelled from the cell after some days. The Trans-IT LT1 kit (Mirus Bio) was used for the transfection of the COS-7 cells. For transfection, the ratio of plasmids was 1:10, with ten times more reporter- and control plasmid, than receptor plasmid (Table 3.5). The transfection reaction mixture (Table 3.6) was incubated at RT for 30 minutes before COS-7 cell growth medium was added. The old medium in the 96-well plates were discarded and replaced with 101.4 µL fresh transfection medium. Cells were then incubated at 37^{o}C, 5 % CO_2 for 24 hr.

Table 3.5: Amounts of plasmids added to each well in the 96-well plate during transfection

Plasmid	Amount [ng]
(MH100)x4 tk luc	47.62
pCMV-β-Gal	47.62
pCMX_GAL4_gmPparx	4.76
Total	100

Table 3.6: Composition of the TransIT-LT1 transfection medium

Component	Amount per well (96-well plate) (µL)
Plasmid mixture [1 µg/ µL]	0.1
OptiMEM w/glutamax	9
TransIT LT1	0.2
DMEM w/ 10 % FBS	92.1
Total	101.4

3.4.5 EXPOSURE TO TEST COMPOUNDS

The transfected COS-7 cells were exposed to test compounds in a seven (14 for WY-14643) concentration dilution series. Test compounds were dissolved in DMSO and serial diluted in exposure medium (Table 2.10 and 3.7) to 2X the exposure concentrations. The concentration of DMSO in exposure wells was 0.5%. The unexposed solvent control used was cell exposure medium containing 0.5 % DMSO. The transfection medium from the 96-well plate was discarded and replaced with 100 µL/well DMEM used for exposure (Table 2.10). Then 100 µL 2X test compound solution was added per well, resulting in a 1X concentration of the test compounds in the plates. The plates were incubated for 24 hr at 37$_{o}$C and 5 % CO_2.

Table 3.7: Compounds used for *in vivo* testing of agonistic effects on gmPparas

Ligand	Highest Conc [µM]	Lowest Conc [µM]	Dilution Factor
WY-14643	200	5.6	1.25
PFOA	267	23	1.5
PFNA	267	23	1.5
PFOS	267	23	1.5

3.4.6 LYSIS AND ENZYMATIC MEASUREMENTS

The exposure was terminated after 24 hr by removing the exposure medium and replacing it with 125 µL lysis reagent solution (Table 2.15) per well. The cells were lysed at RT for 30 min on a platform shaker. During lysis the cell membrane is disrupted to release the luciferase and β-gal enzymes from the cells. 50 µL lysate was transferred to a clear absorbance 96-well plate

for measuring of β-gal activity, while 50 µL of lysate was transferred to a white luminescence 96-well plate for measuring of luciferase activity.

For measurements of β-gal enzyme activities a β-gal reaction solution (Table 2.17) was prepared. To each well, 100 µL β-gal reaction solution was added. This was incubated for approximately 20 min, when the yellow color from the produced ONP appeared. The amount of ONP was measured as absorbance at 420 nm using the EnSpire 2300 Multimode Reader (PerkinElmer). For luciferase activity measurements a luciferase reaction solution (Table 2.19) was prepared. To each well, 100 µL were added and the measurements performed immediately. Luciferase activity was measured as emitted light with the EnSpire 2300 Multimode Reader (PerkinElmer). The recorded luciferase activities were adjusted for differences in transfection efficiencies by dividing luciferase activities with the corresponding β-gal activities using Microsoft Excel, and the activation profiles visualized using non-linear regression in GraphPad Prism.

3.5 VIABILITY/CYTOTOXICITY ASSAY

A viability assay was performed to assess if the test compounds used in LRA were toxic for the COS-7 cells. The viability assay was conducted with the same experimental conditions used in the LRA. A combination of two fluorometric assays, resazurin, and 5-carboxyfluorescein diacetate acetoxymethyl ester (CFDA-AM) were used to assess membrane integrity and metabolic activity. Resazurin is cell permeable and non-fluorescent. Within metabolic active cells it gets reduced by oxidoreductases to the fluorescent compound resorufin, measuring the metabolic activity in the COS-7 cells (Pace & Burg, 2015; H. X. Zhang, Du, & Zhang, 2004). CFDA-AM is also cell permeable and non-fluorescent. Within the cells CFDA-AM is hydrolyzed to fluorescent 5-carboxyfluorescein by intracellular esterases, and because only cells with the plasma membrane intact can maintain esterase activity this assay measures the integrity of the membrane (Bopp & Lettieri, 2008; Schreer, Tinson, Sherry, & Schirmer, 2005).

Cells were seeded in 96-well plates as described in section 3.4.3. Samples were prepared in triplicates. After incubation, old media was discarded and replaced with 101.4 µL medium (Table 2.10). The cells were incubated for 24 hr, at 37 ^{o}C, 5 % CO_2. The exposure was conducted as in LRA (3.4.5). After 24 hr exposure the medium was discarded, and the cells washed with 100 µL 1XPBS per well. The viability reaction solution (Table 2.24) was added

100 µL/well, and incubated at 37 ^{o}C, 5 % CO_2 for 1 hr. Fluorescence were measured with EnSpire 2300 Multimode Reader (PerkinElmer) at 530/590 nm for resazurin and 485/530 nm for CFDA-AM.

3.6 Sodium Dodecyl Sulfate Polyacrylamide Gel Electrophoresis (SDS-PAGE) and Western Blotting

Sodium dodecyl sulfate polyacrylamide gel electrophoresis (SDS-PAGE) is a method for separating proteins according to their size. Prior to the electrophoresis, proteins are denatured by boiling at 95^{o}C in a sample buffer. The sample buffer contains a reducing agent (β-mercaptoethanol) that breaks disulfide bonds in proteins, in addition to the anionic detergent sodium dodecyl sulfate (SDS). SDS binds to the proteins, promoting denaturation and coating the polypeptide chain, providing the proteins with an overall negative charge. The proteins will then be separated according to their mass-to-charge ratio. Where smaller proteins migrate faster through the gel, and larger protein migrate slower because of more resistance in the gel.

3.6.1 Preparation of cell lysates for protein analysis

COS-7 cells were seeded in 96-well plates (Section 3.4.4) and transfected (3.4.5). After 24 hr, old medium was discarded, and the cells washed with 100 µL 1X PBS per well. Subsequently, the cells were lysed with 20 µL lysis reagent per well (Table 2.26) and incubated on ice while shaking for five min. The lysate was pooled from 8 replicate wells and stored at -80^{o}C.

3.6.2 Sodium Dodecyl Sulfate Polyacrylamide Gel Electrophoresis (SDS-PAGE)

The MINI-PROTEAN Tetra Cell (Bio-Rad) was used for SDS-PAGE. Two gels were casted 0.75 mm thick. One gel was used for protein immunoblotting, and one gel was used for protein staining with Coomassie Brilliant Blue. Each gel consisted of a 10 % separation gel, and a 4 % stacking gel (Table 2.27) casted on top of the separation gel. When the gels had polymerized, they were transferred from the casting unit to an electrophoresis chamber. The chamber was filled with 1X TGS buffer (Table 2.28). A Precision Plus Protein™ Prestained Protein Standards (Bio-Rad) was used as a protein size marker, and 5 µL of each protein sample was loaded in the wells of the gel. The gel was run for 45 min at 200 V.

3.6.3 Total Staining of Proteins in using Coomassie Brilliant Blue

For evaluation of the total protein content in the SDS-PAG, one gel was stained with Coomassie Brilliant Blue R250 staining solution with InstantBlue™ Coomassie Protein Stain (Expedeon) ON shaking at RT. The gel was rinsed with ddH_2O for destaining. A picture was taken with ChemiDoc XRS+ (Bio-Rad).

3.6.4 Protein Immunoblotting

Protein immunblotting is an antibody-based method for the detection of specific proteins, and was used to assess the synthesis of gmPpar wts and mutants in the COS-7 cells. For protein immunoblotting the Mini Trans-Blot Electrophoretic Transfer Cell was prepared and used. A PVDF-membrane (6*9 cm) was activated by submerging in methanol for 20 sec, rinsed in dH_2O, and soaked in transfer buffer for 10-15 min together with filter papers and sponges for the blotting sandwich. The sandwich was placed in an electrophoresis chamber together with a cooling unit. The chamber was filled with transfer buffer (Table 2.29), and the electroblotting was conducted for 1 hr at 100 V. The membrane was blocked ON in 5 % dry-milk in TBS-tween (TBS-T) (Table 2.32) at 4 ^oC on a platform shaker. The dry-milk was washed away with TBS-T the next day (Table 2.31). Primary anti-GAL4-DBD antibody (Table 2.33) was diluted 500 times in TBS-T and incubated on the membrane for 1 hr at RT while shaking. The membrane was washed in TBS-T to remove excess antibodies. The secondary antibody anti-mouse IgG (Table 2.33) was diluted 1:2000 in 10 mL TBS-T and incubated on the membrane for 1 hr while shaking. Excess antibody was removed by washing with TBS-T. A second wash was performed with TBS buffer (Table 2.30). To visualize the immunoreactive proteins, the SuperSignal™ West Femto Maximum Sensitivity Substrate kit was used. A working solution of 2 mL was prepared and used according to the manufactures protocol. The bands were visualized with the ChemiDoc XRS+ (Bio-Rad).

β-actin was used as a loading control since it is expressed in all eukaryotic cell types. To blot for beta-actin the membrane was washed with TBS-T. Then a primary antibody specific for β-actin (Table 2.33) was diluted 1000 times in 10 mL TBS-T and incubated on the membrane for 1 hr while shaking. The primary antibody was discarded and replaced with secondary antibody (Table 2.33) and incubated for another hour while shaking. The bands were visualized using the kit SuperSignal West Pico Chemiluminescent and the procedure described above.

3.7 AGAROSE GEL ELECTROPHORESIS

Agarose gel electrophoresis (AGE) is a method used to separate and visualize nucleic acids. Since nucleic acids are negatively charged they will migrate towards the positive pole through the gel when applying a current, which is carried by the ions in the running buffer. In this work, AGE was used to analyze PCR-products, or to assess plasmid DNA conformation. The agarose gel is added GelRed which interacts with the nucleic acids and allows visualization of DNA or RNA in the gel.

A 0.7 % agarose solution was prepared with 0.5 X TBE buffer (Table 2.12). A gel with 30 mL agarose solution and 0.5 µL GelRed was prepared. This was left for solidification for approximately 20 min at RT. The gel was transferred to an electrophoresis chamber and soaked in 0.5 X TBE buffer. A 2-log DNA ladder was used as a size marker. In every run, 500 ng ladder and sample were loaded onto the gel, and the gels were run at 110 V for 30 min. The gels were visualized with ChemiDoc XRS+ (Bio-Rad).

3.8 SANGER SEQUENCING

For DNA sequencing, the Protocol BigDye v.3.1 kit was used. The reaction mixture was prepared (Table 3.8), and the amplification reaction performed (Table 3.9). After the reaction, 10 µL DI-H_2O was added to each reaction and submitted to the DNA Sequencing Facility at the Department of Biological Sciences, University of Bergen.

Table 3.8: Reaction setup for one sequencing reaction.

Reagent	Quantity
Big-Dye version 3.1	1 µl
Sequencing buffer	1 µl
Template	225 ng
Primer	3.2 pmol
ddH_2O	Total 10 µl

Table 3.9: Thermal cycle program for the sequencing reaction.

Step	Cycles	Time	Temp. [$_oC$]
1	1	5 min	96
2	34	10 sec	96
		5 sec	50
		4 min	60
3		∞	4

4. RESULTS

The main aim of this study was to investigate if structural differences originating from deviations in the AA sequence between gmPpara1 and gmPpar2 could contribute to the previously observed differences in activation profiles of the two wt gmPpara subtypes, including the observed discrepancies in activation when exposed to PFASs. To do so, four different mutants of gmPpar2 were constructed in order to make the primary structure more similar to the primary structure of gmPpara1. These resulting mutants were functionally characterized in a GAL4-UAS based LRA with selected agonists to study putative changes in the activation profiles by comparing the wt gmPpars and the constructed mutants.

4.1 Construction and Sequencing of gmPPARA2 Mutants

4.1.1 SDM Deletion in the hinge region of gmPPARA2

The construction of the gmPpara2 mutants was based on a previously constructed plasmid encoding the wt gmPpara2 constructed previously (Söderström, 2017). Appropriate primers were designed and the SDM deletion experiment was performed as described in 3.2.3. Potential mutant plasmids were propagated in *E. coli*, purified, and subsequently sequenced to confirm if the desired 14 AA sequence was deleted from the hinge region of gmPpara2. In Figure 4.1, a multiple sequence alignment (MSA) of the deduced AA sequences after the SDM deletion experiment is shown. The MSA confirmed that the targeted region encoding AAs 266-279 had been deleted in two of the four plasmids. These plasmids were denoted gmPpara2_DEL-1 and gmPpara2_DEL-4, and gmPpara2_DEL-4 was used in the further work.

Figure 4.1: Multiple sequence alignment of the gmPpara2_DEL constructed mutants. After SDM was performed, the plasmids were purified and sequenced at the Sequencing Facility at the Department of Biological Sciences, University of Bergen. The alignment of the translated plasmid sequences covering the relevant region was translated *in silico* using the ExPasy translate tool. Clustal-Omega (EMBL-BI) was used to align the sequences. The alignment was colored in Jalview according to AA percentage identity. The area where the deletions were made is boxed in red.

4.1.2 SDM Amino Acid Substitution in gmPpara2_DEL

gmPpara2_DEL-4 was further used for generating the mutants containing single AA substitutions in addition to the deleting the 14 AAs in the hinge region. Three different mutants were constructed, and hence, three different SDM experiments were performed with appropriate primers specifically designed for each experiment. Sequencing confirmed the successful construction of the mutants, which were denoted as: gmPpara2_DEL_G278>R278, gmPpara2_DEL_L286>H286 and gmPpara2_DEL_G278>R278+L286>H286.

In Figure 4.2A the MSA for the first constructed mutant, gmPpara2_DEL_G278>R278, is shown. All of the sequenced plasmids contained the desired substitution, where G266 had been changed to R266. For the further work gmPpara2_DEL_G>R-1 was chosen.

In Figure 4.2B the MSA for the second constructed mutant, gmPpara2_DEL_L286>H286, is shown. The mutant gmPpara2_DEL_L286>H286 was constructed with the same approach as in the G278>R278 SDM experiment. The MSA show that all plasmids had been mutated successfully, and L286 had been changed to H286. gmPpara2_DEL_L286>H286-1 was used in the further work.

Figure 4.2C shows the MSA for the third constructed mutants. The double mutant gmPpara2_DEL_G278>R278+L286>H286 was created with the same procedure as used for the SDM single AA substitution mutants, except that two mutagenic primer pairs were used simultaneously. The MSA show that G278 was mutated to encode R278 in plasmid two and four, while L286 had been changed to encode H286 in plasmids one, three, and four. Thus, the only successfully constructed mutant with both mutations present was plasmid number 4. gmPpara2_DEL_G278>R278+L286>H286-4 was accordingly chosen for further work.

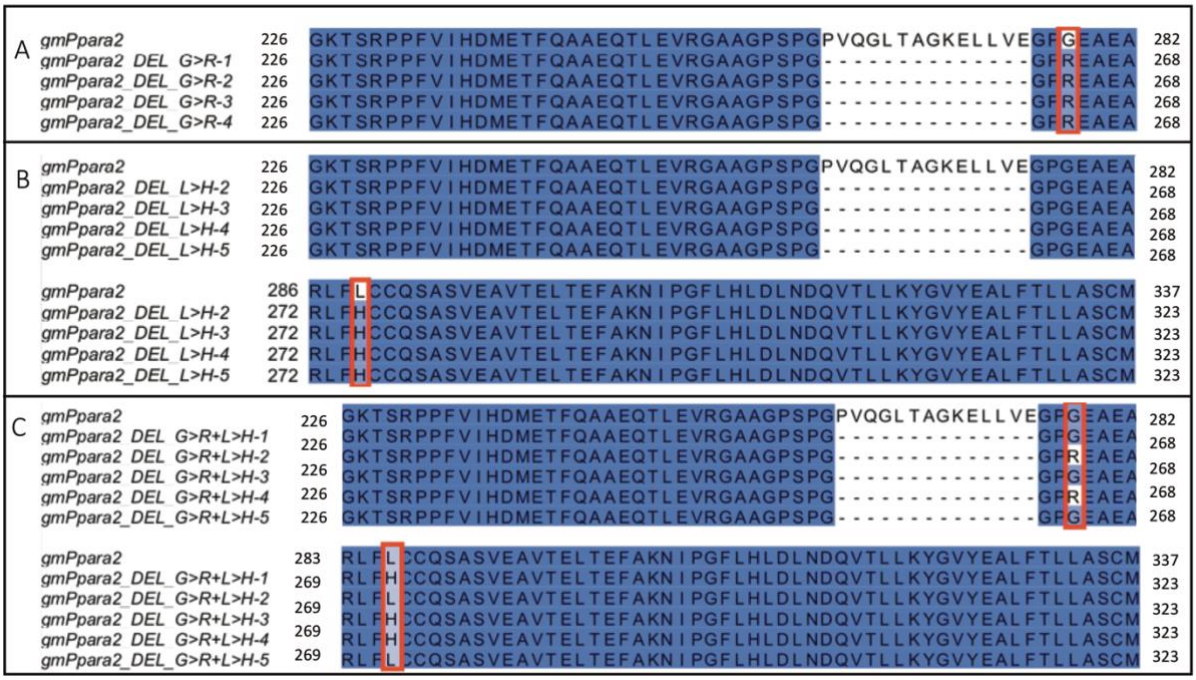

Figure 4.2: Multiple sequence alignment demonstrating the amino acid substitutions made by SDM in gmPpara2_DEL. Three different SDMs were performed, and the plasmids were purified and sequenced at the Sequencing Facility at the Department of Biological Sciences, University of Bergen. Translations of AAs in the regions of interest were aligned in ClustalOmega (EMBL-BI), and the alignments were visualized in Jalview according to percentage identity. AAs targeted for substitutions have been indicated with red boxes. Alignment A shows the resulting plasmid from SDM of the gmPpara2_DEL_G278>R2787. Alignment B show the gmPpara2_DEL_L286>H286 SDM. Alignment C show the gmPpara2_DEL_G278>R278+L286>H286 SDM.

4.1.3 Overview of the wt gmPparas and the constructed mutants

An MSA of the hinge and LBD regions demonstrate the differences in the AA sequences between gmPpara1, gmPpara2, and the constructed gmPpara2 mutants (Fig. 4.3). Both the deleted stretch of 14 AAs and the single AA substitutions were located in the hinge region of the receptor (yellow line). Furthermore, the conserved AAs in the LBD-region (green line) important for binding of the WY-14643 model-agonist in the canonical binding site are highlighted in the MSA. The AAs important for binding of WY-14643 in the second allosteric binding site in hPPARa are also highlighted.

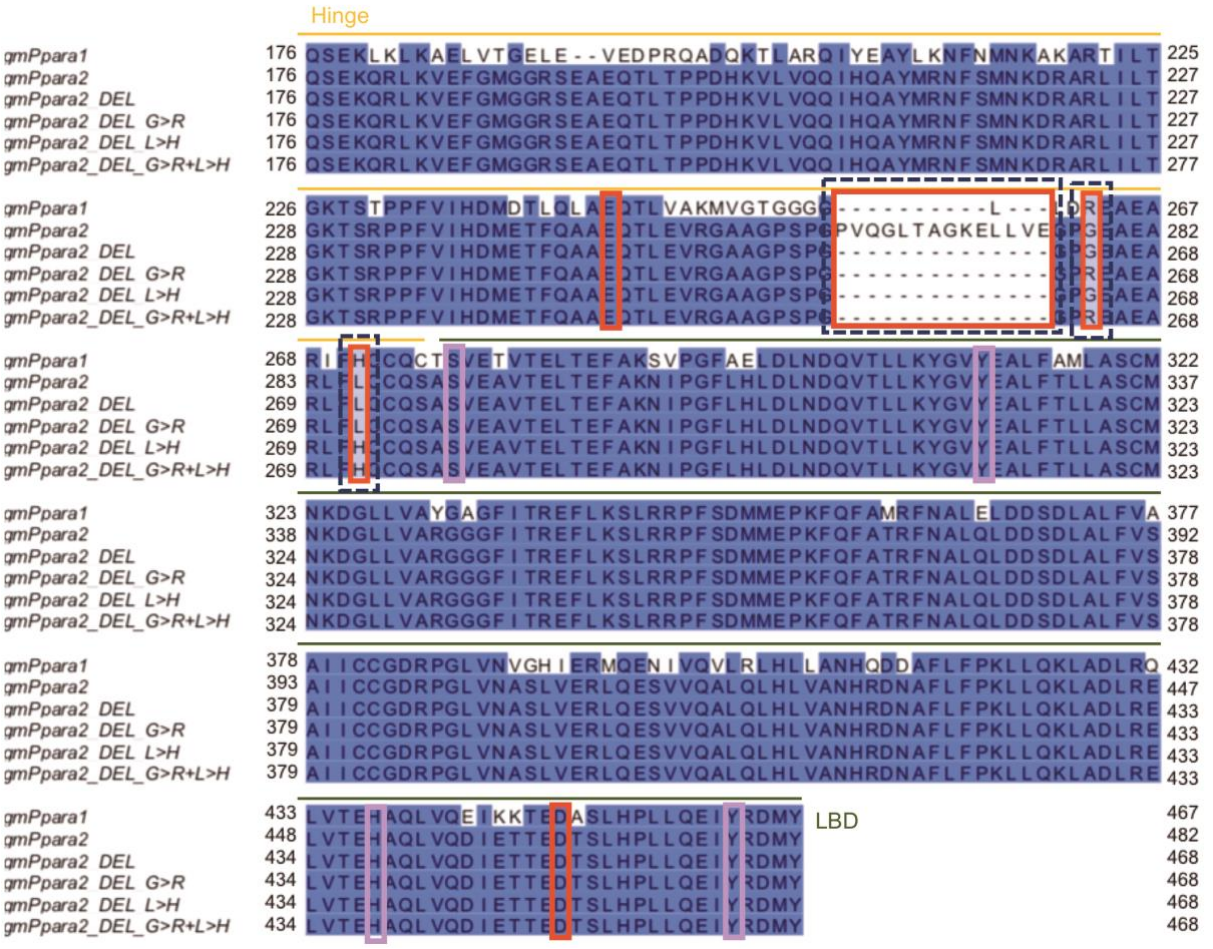

Figure 4.3: Multiple sequence alignment of wild type and mutated Atlantic cod gmPpars. Plasmids encoding fusion proteins of GAL4-DBD and wild type gmPpara1 and gmPpara2, as well as mutant plasmids, were sequenced at the Sequencing Facility at the Department of Biological Sciences, University of Bergen and translated into protein sequences *in silico* using the ExPasy translate tool. The sequences were aligned with Clustal Omega (EMBL-EBI). Jalview was used to visualize the alignment according to percentage AA identity. Conserved AAs important for binding of WY-14643 in the canonical binding site in hPPARa are marked with pink boxes. The extended stretch of AAs in the hinge region of gmPpara2, and AAs that constitute the second binding site for WY-14643 in hPPARa are marked in red. The mutations that were made are indicated with dotted lines. The hinge region and LBD is indicated on top of the alignment in yellow and green lines, respectively.

4.2 TRANSACTIVATION ANALYSES OF GMPPARAS AND GMPPARA MUTANTS

4.2.1 PLASMID INTEGRITY CONTROL PRIOR TO LRA

Plasmid integrity may affect the transfection-efficiency into mammalian cell lines. The plasmid integrities were therefore assessed with agarose gel electrophoresis prior to use in the LRA (Fig. 4.4). The majority of the plasmids were present in the fastest migrating band in the gel, indicating that most plasmids were in the supercoiled conformation preferable for later transfection into COS-7 cells. The two less predominant higher molecular weight bands in the gel most likely represent plasmids in the circular nicked and linear conformation, respectively. Importantly, these results indicated that the plasmids in all preparations were largely supercoiled and suitable for transfection.

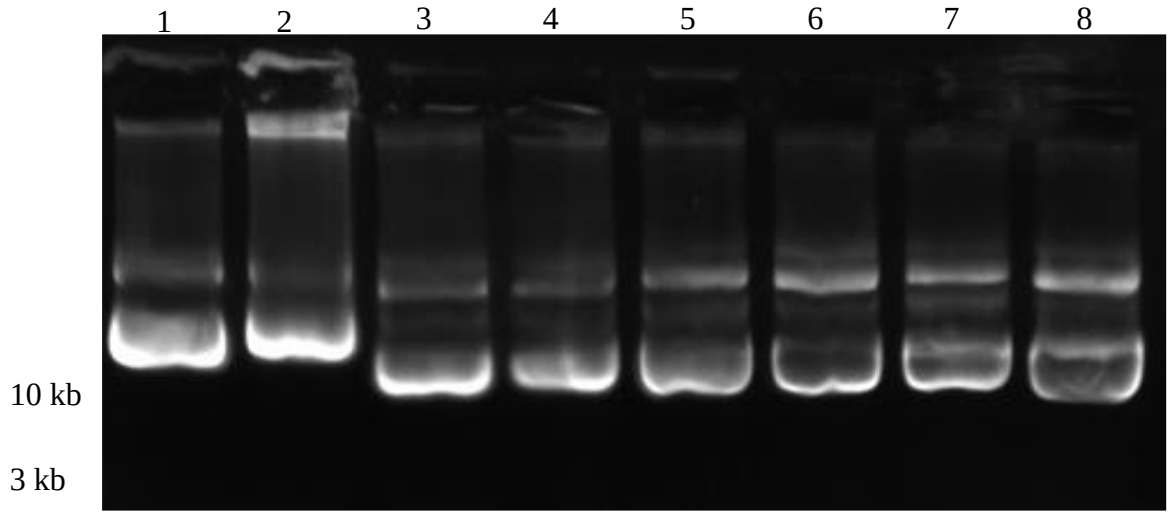

Figure 4.4: Assessment of the conformation of plasmids used for LRA. Purified plasmids were separated in a 0.7 % agarose 0.5X TBA gel for 30 min at 200 V. 500 ng of each plasmid sample was applied to the gel. Reporter plasmid ((MH100)x4tk-luciferase (**lane 1**)), control plasmid (pCMV-β-galactosidase (**lane 2**)), and receptor plasmids, (pCMX_GAL4_gmPpara1 (**lane 3**), pCMX_GAL4_gmPpara2 (**lane 4**), pCMX_GAL4_gmPpara2_DEL (**lane 5**), pCMX_GAL4_gmPpara2_DEL_G>R (**lane 6**), pCMX_GAL4_gmPpara2_DEL_L>H (**lane 7**) and pCMX_GAL4_gmPpara2_DEL_G>R+L>H (**lane 8**)), 500 ng of each plasmids and a 2-LOG ladder (New England Biolabs) was applied in each well.

4.2.2 EVALUATION OF EXPRESSION OF GMPPARS AND GMPPAR MUTANTS IN COS-7 CELLS

To confirm the translation and production of the GAL4_gmPpara fusion proteins in the COS7 cells (both wt and constructed mutants), SDS-PAGE and protein immunoblotting were performed (Methods 3.6). Forty-eight hours after seeding, and 24 hours after transfection, the cells were harvested and lysed as described in 3.6.1. The cell lysates were separated with SDS-

PAGE according to their MW. One parallel gel was Coomassie-stained to verify proper separation of the polypeptides and to visualize total protein content (Fig. 4.5A). The other gel was used for protein immunoblotting for detection of the GAL4-gmPparx fusion proteins using an anti-GAL4-DBD antibody (Table 2.33), (Fig. 4.5B). The expression of β-actin was used as a loading control and was detected using an anti-β-actin antibody (Fig. 4.5C) (3.6.4). The Coomassie-stained gel showed that the proteins were separated successfully during the electrophoresis, and indicated that similar amounts of protein was applied in each well (Fig. 4.5A). The membrane used for immunoblotting was first probed with the primary anti-GAL4 antibody in the first round of blotting, and anti-β-actin in the second round of blotting (3.6.4). The fusion proteins, including gmPpara1, gmPpara2, gmPpara2_DEL, gmPpara2_DEL_G>R, gmPpara2_DEL_L>H, and gmPpara2_DEL_G>R+L>H were detected as immunoreactive bands around 50 kDa in cell lysates prepared from the transfected COS-7 cell (Fig. 4.5B). The wt gmPpara2 (GAL4-DBD-gmPpara2-hinge+LBD) appear to migrate slower in the PA-gel, which corresponds well to their predicted MWs (Table 4.1). As expected, no immunoreactive bands were detected in the non-transfected cells using the anti-GAL4-DBD antibody, demonstrating that gmPpara-proteins were only expressed in COS7 cells transiently transfected with plasmids encoding GAL4-gmPpara fusion proteins. β-actin was detected in all samples around 42 kDa in both untransfected and transfected cell lysates.

Table 4.1: The predicted MWs of gmPparx fusion proteins

Receptor	Theoretical Mw (kDa)
GAL4-DBD-gmPpar1-hinge+LBD	50.2
GAL4-DBD-gmPpara2-hinge+LBD	51.5
GAL4-DBD-gmPpara2_DEL-hinge+LBD	50.3
GAL4-DBD-gmPpara2_DEL_G>R-hinge+LBD	50.2
GAL4-DBD-gmPpara2_DEL_L>H-hinge+LBD	50.2
GAL4-DBD-gmPpara2_DEL_G>R+L>H-hinge+LBD	50.2

The MWs have been predicted using the ExPASy Compute pI/MW Tool.

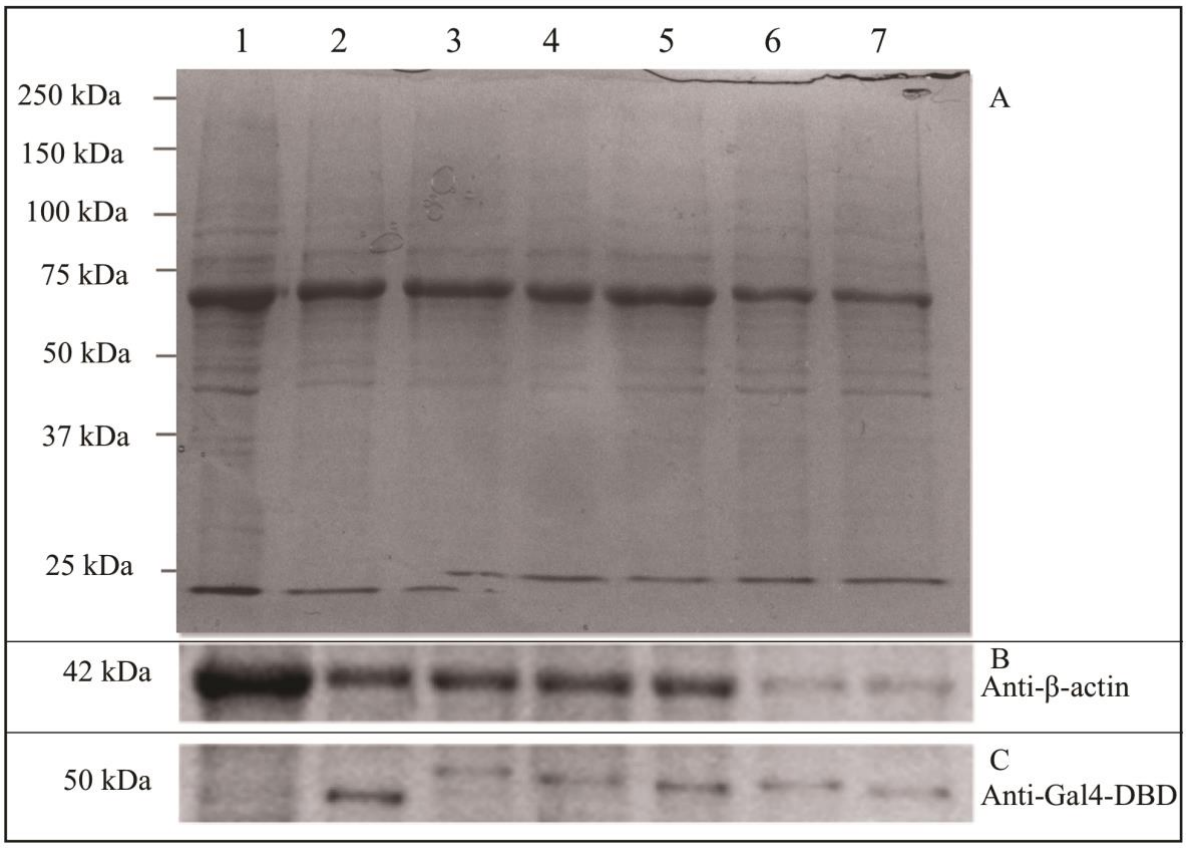

Figure 4.5: Detection of the fusion proteins GAL4-gmPpars in transfected COS-7 cells with protein immunoblotting. The COS-7 cell lysates were separated on two 10 % PA gels. (**A**) SDS-PAG stained with Coomassie Brilliant Blue. The corresponding PVDF-membrane were treated with (**B**) mouse anti-GAL4 (diluted 1:500 in TBS-Tween) and sheep-anti-mouse-IgG (diluted 1:2000 in TBS-Tween), and (**C**) with mouse anti-β-actin and sheep-anti-mouse-IgG. **Lane 1:** untransfected COS-7 cells. COS-7 cells were transfected with the following receptor plasmids; pCMX_GAL4_gmPpara1 (**lane 2**), pCMX_GAL4_gmPpara2 (**lane 3**), pCMX_GAL4_gmPpara2_DEL (**lane 4**), pCMX_GAL4_gmPpara2_DEL_G>R (**lane 5**), pCMX_GAL4_gmPpara2_DEL_L>H (**lane 6**) and pCMX_GAL4_gmPpara2_DEL_G>R+L>H (**lane 7**). As a size marker, the Precision Plus Protein™ Kaleidoscope ™ Prestained Protein Standard from Bio-Rad was used.

4.2.3 Activation of wt gmPPARs and gmPPAR mutants exposed to various agonists

Initially, the activation of the wt gmPpara1 and gmPpara2 by the WY-14643 model agonist was investigated with the GAL4-UAS based LRA assay. Exposure of COS-7 cells expressing gmPpara1 to increasing concentrations of WY-14643 produced a dose-dependent increase in luciferase activity to a maximum level of 23.6-fold higher than solvent-exposed cells ($p \leq 0.0001$) (Fig. 4.6, Table 4.2). In cells expressing gmPpara2, the maximum increase in luciferase activity was 8.8-fold ($p \leq 0.046$) after WY-14643 exposure (Table 4.2). The EC_{50} values for gmPpara1 and gmPpara2 were estimated to be 56.5 μM (53.4-60.0, 95% CI) and 97.5 μM (92.4-103.8, 95% CI), respectively (Table 4.3).

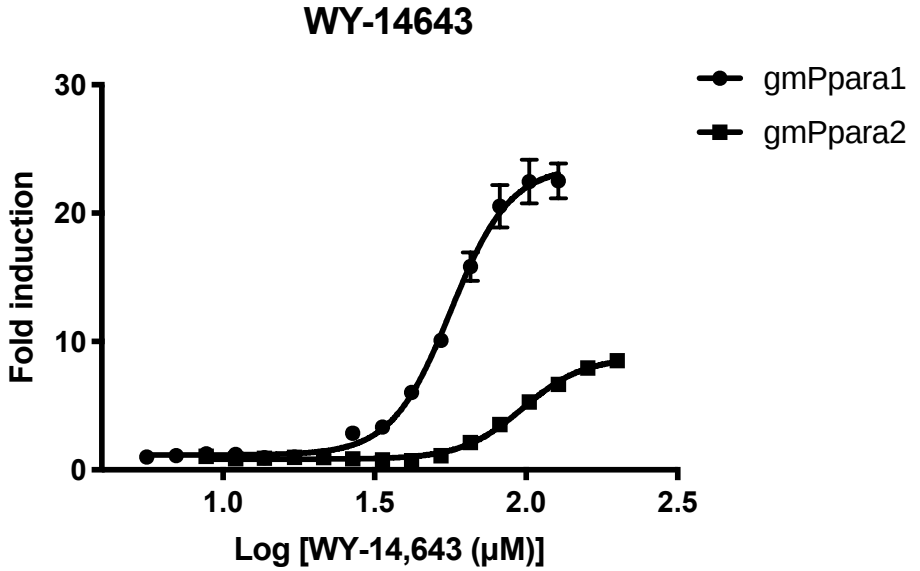

Figure 4.6: Activation of gmPpara1 and gmPpara2 by WY-14643. COS-7 cells were co-transfected with the receptor plasmids (gmPpara1 or gmPpara2), reporter plasmid ((MH100)x4tk-luciferase) and control plasmid (pCMV-β-galactosidase). After transfection cells were exposed to increasing concentrations of WY-14643 for 24 hr. The activation of the GAL4-gmPpara1/a2 receptor is shown as relative fold change in luciferase activity in WY-14643-exposed cells compared to the solvent exposed cells (0.5 % DMSO). Three individual experiments were performed, each with exposures in triplicates (n=9). The dose-response curves were fitted by non-linear regression (GraphPad, PRISM v7.0).

4.2.4 Activation of wt and mutated gmPPARs when exposed to WY-14643

The GAL4-UAS-based LRA was also used to assess the effect of the mutations on the activity of gmPpara2 when exposed to WY-14643 and a selected set of PFASs. Comparison of activation profiles of gmPpara2 mutants and wt gmPpara2 when exposed to WY-14643 demonstrated several differences (Fig. 4.7). In general, the response mediated by the gmPpara2 mutants was much stronger (higher efficacy) than responses mediated by the wt gmPpara2 (Fig. 4.10A, Table 4.2). The constructed mutants had a distribution of their maximum fold activation between 171- and 134-fold induction, in the following order: gmPpara2_DEL > gmPpara2_DEL_G>R+L>H > gmPpara2_DEL_G>R > gmPpara2_DEL_L>H (Table 4.2). In comparison, activation of the wild type gmPpara2 reached a maximum of approximately 9-fold. All of the constructed mutants had at least 15 times stronger activation than gmPpara2, and 6 times stronger activation than gmPpara1. The calculated EC_{50}-values (Table 4.4) demonstrated that WY-14643 was a significantly more potent agonist to different gmPpara2 mutants (Table 4.5) compared to the wt gmPpara2, except for the mutant gmPpara2_DEL_L>H. However, WY-14643 was the most potent agonist for gmPpara1, which produced the lowest EC_{50} value. The potency of WY-14643 towards the gmPpara2 mutants were mostly not statistically different from each other. Although the responses of the wt and constructed mutants were different regarding magnitude (efficacy, Emax) and EC50, the activation of the receptors all starts at relatively low and similar concentrations of WY14643, as illustrated by LOECs ranging between 9-27 μM (Fig. 4.7 A, Table 4.4). The E_{max}-values determined for the receptors can be statistically grouped into three (Table 4.3): 1) The maximum response for all constructed mutants were significantly different from that of wt gmPpara2. 2) The maximum response of gmPpara2_DEL was significantly different from all three mutants containing the additional single or double AA-substitutions. 3) The three mutants containing the single or double AA substitutions did not have significantly different E_{max}-values from each other. The EC_{50} values of the different gmPpara2 mutants were statistically different from wt gmPpara2 (Table 4.4, Table 4.5), and the mutants had EC_{50} values in the range between gmPpara1 and gmPpara2. Moreover, the EC_{50} values of gmPpara2_DEL_G>R and the EC_{50} value of gmPpara2_DEL_L>H were significantly different from each other. None of the other EC_{50} values of the constructed mutants were significantly different from each other (Table 4.5).

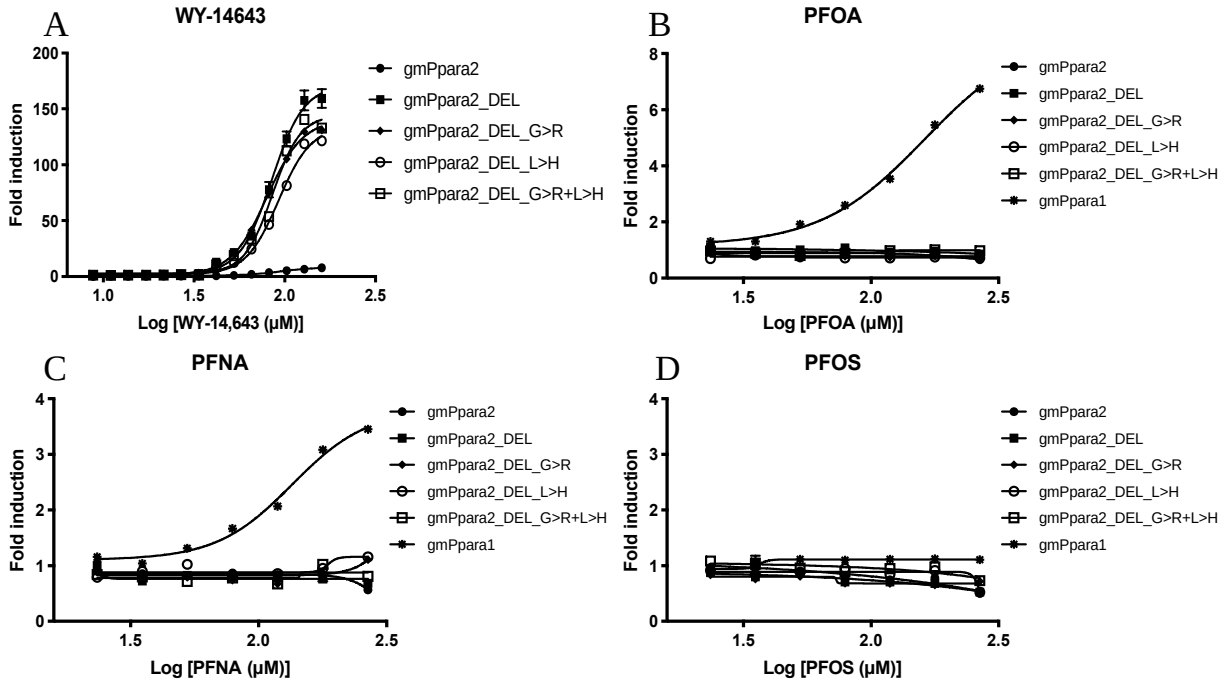

Figure 4.7: Activation profiles for different wt and mutant gmPpars exposed to WY-14643, PFOA, PFNA and PFOS. The dose-response curves (A-D) show the activation profiles of gmPpars exposed to WY-14643 and three selected PFASs, including PFOA, PFNA, and PFOS. COS-7 cells were seeded and co-transfected with the receptor plasmids (gmPpara1, gmPpara2, gmPpara2_DEL, gmPpara2_DEL_G>R, gmPpara2_DEL_L>H, or gmPpara2_DEL_G>R+L>H), reporter plasmid ((MH100)x4tk-luciferase) and control plasmid (pCMV-β-galactosidase). After transfection cells were exposed to increasing concentrations of the different test compounds as indicated for 24 hr. Activation of GAL4-gmPpars is shown as fold change in luciferase activity in exposed cells compared to cells exposed to solvent control (0.5 % DMSO). Each experiment was performed three times, with three technical replicates (n=9). Non-linear regression (GraphPad, Prism) was used to create the dose-response the curves.

4.2.5 Activation of wt and mutated gmPparas when exposed to PFOA, PFNA and PFOS

PFOA and PFNA induced a 7.6-fold ($p<0.0001$) and a 2.7- fold ($p<0.0001$) activation of gmPpara1, respectively, when compared to the solvent control (Fig. 4.7 B and C, Table 4.1). EC_{50}-values were not estimated since a stable plateau of activation was not reached. For gmPpara2 and the constructed gmPpara2 mutants, no activation was observed by either PFOA or PFNA. PFOS did not activate any of the wt gmPpars or the constructed mutants (Fig. 4.7 D). For PFNA and PFOS an apparent decrease in the luciferase signal at the higher concentrations used were observed.

Table 4.2: Maximum response (E_{max}) and lowest observed effect concentration (LOEC) produced by WY-14643.

		Maximum response (E_{max})			Lowest observed effect concentration (LOEC)		
Receptor	**Test compound**	**Conc. [µM]**	**Fold, 95 % CI**	**p-value**	**Conc. [µM]**	**Fold ± SD**	**p-value**
gmPpara1	WY-14643	128	23.6, 22.2-25.4	<0.0001	26.8	2.9	<0.0001
	PFOA						
gmPpara1	PFNA	267	7.6, 6.0-?	<0.0001	23.4	1.3	0.015
gmPpara1		267	2.7, 3.3-?	<0.0001	52.7	1.3	0.002
gmPpara2	WY-14643	160	8.8, 8.2-9.4	<0.0001	11.0	0.9	0.046
gmPpara2_DEL	WY-14643	128	171.1, 161.2-183.4	<0.0001	13.7	1.3	0.0035
gmPpara2_DEL _G>R	WY-14643	160	140.6, 130.2-154.6	<0.0001	17.2	1.4	0.026
gmPpara2_DEL _L>H	WY-14643	160	134.1, 124.0-148.6	<0.0001	21.5	1.3	0.048
gmPpara2_DEL _G>R+L>H	WY-14643	160	144.5, 137.0-153.7	<0.0001	8.9	1.2	0.0007

Table 4.3: Statistical differences in E_{max} between gmPparas exposed to WY-14643.

	gmPpara2	gmPpara2_DEL	gmPpara2_DEL_G>R	gmPpara2_DEL_L>H
gmPpara2_DEL	<0.001			
gmPpara2_DEL_G>R	<0.001	<0.001		
gmPpara2_DEL_L>H	<0.001	<0.001	0.998	
gmPpara2_DEL_G>R+L>H	<0.001	<0.001	>0.999	0.961

A one-way ANOVA and Sidaks multiple comparisons test was used to test for statistical significance.

Table 4.4: EC_{50} values for gmPpars activated by WY-14643, PFOA and PFNA.

Receptor	Agonist	Half maximal Effective concentration 50 (EC_{50} (µM), + 95 % CI)
gmPpara1	WY-14,643	56.5, 53.4-60.0
gmPpara2	WY-14643	97.5, 92.4-103.8
gmPpara2_DEL	WY-14643	84.8, 81.4-88.9
gmPpara2_DEL_G>R	WY-14643	79.6, 75.1-85-5
gmPpara2_DEL_L>H	WY-14643	92.3, 87.7-98.7
gmPpara2_DELG>R+L>H	WY-14643	85.5, 82.4-89.0

Table 4.5: Statistical differences in EC_{50} between gmPparas exposed to WY-14643.

	gmPpara2	gmPpara2_DEL	gmPpara2_DEL_G>R	gmPpara2_DEL_L>H
gmPpara2_DEL	0.004			
gmPpara2_DEL_G>R	<0.001	0.832		
gmPpara2_DEL_L>H	0.912	0.363	0.003	
gmPpara2_DEL_G>R+L>H	0.011	>0.999	0.678	0.580

A one-way ANOVA and Sidaks multiple comparisons test was used to test for statistical significance.

4.2.6 Cytotoxic effects in COS-7 cells after exposure to test compounds

To monitor if any of the PFASs used in the LRA were cytotoxic, and hence affected the viability of the COS-7 cells, the effects of the test compounds (PFOA, PFNA and PFOS) on the cells metabolic activity and membrane integrity were assessed. In a previous study it was shown that WY-14643 did not affect COS-7 viability, hence the cytotoxicity test was not repeated in this thesis (Söderström, 2017). In Figure 4.8, the measured metabolic activities (4.8 A-C), and the plasma membrane integrities (4.8 D-F) are shown. As expected, COS-7 cells exposed to 0.5 % Triton X-100 (used as a positive control) showed a distinct reduction in metabolic activity to 8 % of non-exposed cells, while plasma membrane permeability was reduced to 2 %. For PFOA, a significant decrease in metabolic activity, as well as a reduction of plasma membrane integrity, were observed for concentrations between 23-267 µM. In COS-7 cells exposed to PFNA, a dose-dependent decrease in metabolic activity was observed for exposures of 79-267 µM, with the viability decreasing from 94 % to 81 %. With regards to plasma membrane integrity, PFNA exposure showed a dose-dependent decrease at exposures of 35-267 µM, with the membrane integrity decreasing from 84 % to 56 %. Similarly, PFOS induced a small dose-dependent decrease in COS-7 cell metabolic activity for concentrations between 53-267 µM,

with the activity decreasing from 93 % to 81 %. PFOS exposure also caused a decrease in the plasma membrane integrity of COS-7 cells.

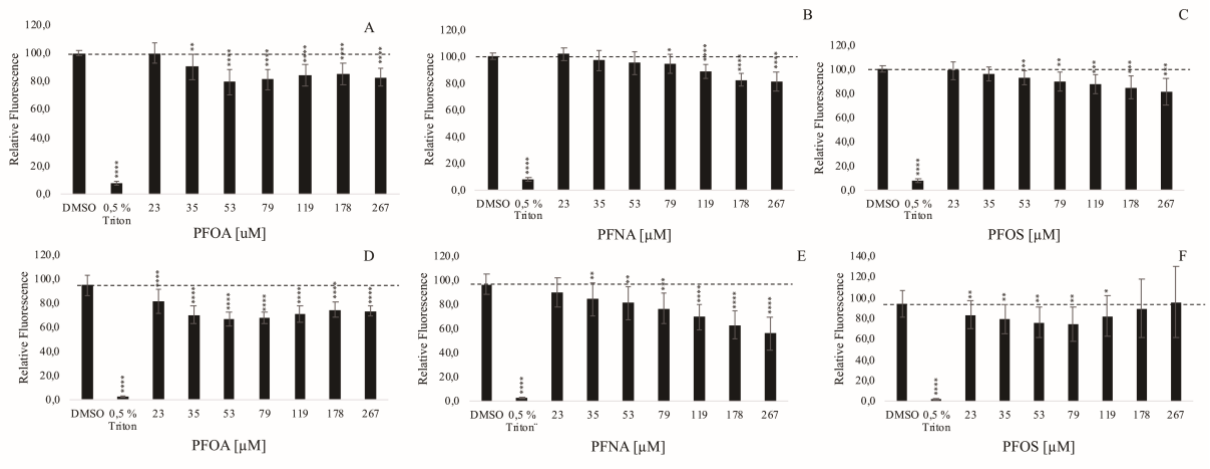

Figure 4.8: Viability of COS-7 cells after exposure to different PFAS. COS-7 cells were exposed to the same range of concentrations of PFOA, PFNA, and PFOS, as used in the LRA. Exposure to DMEM with 0.5 % DMSO (solvent control) or 0.5 % Triton X-100 were used as a negative and positive control for cytotoxicity, respectively. Cytotoxic responses were defined as a decrease in the fluorescent signal compared to the cells exposed to 0.5 % DMSO, which was defined as 100 % and indicated as a dotted line in the graphs. (A-C) Upper panels show the metabolic activity using resazurin measurements. (D-F) Lower panels show the plasma membrane integrity as measured by CFDA-AM. Significance is indicated as * = $p \leq 0.05$, ** = $p \leq 0.01$, *** = $p = \leq 0.001$, **** = $p \leq 0.0001$, calculated using a TTEST.

5. DISCUSSION

The family of PPAR receptors has been found to be key regulators of the lipid homeostasis, energy utilization and lipid storage, with three different main subtypes found in vertebrates, i.e. PPARa, PPARd, and PPARg (Desvergne & Wahli, 1999). Some teleosts, including Atlantic cod, possess two Ppara subtypes, denoted Ppara1 and Ppara2 (Bertrand et al., 2007; Maglich et al., 2003; Metpally et al., 2007) This thesis has focused on the Atlantic cod gmPpara1 and gmPpara2. Notably, the gmPpara1 receptor was previously shown to be activated by some PFASs, including PFOA, PFNA and PFHxS. The Atlantic cod Ppara2 was not activated by any of these compounds. Moreover, both a lower efficacy and a lower potency of the control agonist WY-14643 on gmPpara2 were observed compared to the gmPpara1 receptor (S.Söderstrøm, 2017). Importantly, distinct differences in the primary structures of gmPpara1 and gmPpara2 have been observed, and the functional implications of some of these differences in regard to ligand recognition and activation have been explored in this thesis.

In this study four different gmPpara2 mutants have been constructed. These mutants, in addition to the wt gmPpara1 and gmPpara2 receptors (Table 2.5), were exposed to the PPARa model-agonist WY-14643 and selected PFASs (PFOA, PFNA and PFOS), and characterized using a luciferase-based reporter gene assay (LRA) in COS-7 cells. This assay was used to investigate the ability of the test compounds to activate the fusion protein GAL4-DBD-gmPparx-hinge+LBD. The synthesis of the fusion proteins in COS-7 cells was examined with SDS-PAGE and protein immunoblotting. The cytotoxicity of the compounds in COS-7 cells was monitored in a cytotoxicity assay.

CONSTRUCTION OF GMPPARA2 MUTANTS AND EXPRESSION IN COS-7 CELLS

The first mutant, gmPpara2_DEL, was constructed based on recent *in silico* modeling data which suggested that the 14 additional AA in the gmPpara2 hinge region contributed to the observed differences in activation profiles of gmPpara1 and gmPpara2 when exposed to WY-14643 and certain PFAS congeners. The mutants with single AA substitutions, in addition to the deletion in the hinge region, were designed based on previous reported results from

hPPARa, suggesting that four AAs, in which two of these differ between hPPARa/gmPpara1 and gmPpara2, play an important role in binding of WY-14643 to a non-canonical second binding site (Bernardes et al., 2013). The first single AA mutated in gmPpara2_DEL was G278, an aliphatic, hydrophobic and non-reactive AA (Petrat, Boengler, Schulz, & de Groot, 2012). G was replaced with R278 a hydrophilic, positively charged AA, which can participate in both hydrophilic and hydrophobic interactions (Armstrong, Mason, Anderson, & Dempsey, 2016). Arginine is also the AA present in this position in the gmPpara1 receptor. The second AA mutated was L286, also an aliphatic, hydrophobic and non-reactive AA (Kathuria, Chan, Nobrega, Özen, & Matthews, 2016). This AA was changed to H286, a basic, positively charged AA (Ingle, 2011), which was present in this position in both the gmPpara1 and the hPPARa. Thus, both the 14 AA deletion and the additional two AA substitutions created gmPpara2 mutants that were more similar to gmPpara1. All of the constructed mutants were successfully constructed with SDM and verified with DNA sequencing.

Protein immunoblotting, using an antibody towards GAL4-DBD, was used to investigate if the gmPpar fusion proteins were produced in the transiently transfected COS-7 cells (Fig.4.2.3). While β-actin was detected in all cell lysates, the GAL4-reactive proteins were only detected in transfected cells, indicating a successful production of the GAL4-DBD-gmPparax-hinge+LBD proteins. Similar amounts of gmPpars were apparent in the different cell lysates, suggesting that the mutations did not significantly affect expression of the gmPpara variants in the COS7-cells.

ACTIVATION OF GMPPARS IN THE LUCIFERASE REPORTER GENE ASSAY

WHY USE THE LUCIFERASE REPORTER GENE ASSAY?

Reporter gene systems have commonly been used as a tool to study ligand-activation of NRs, as the expression of the reporter gene is a direct result of receptor activation (Paguio, Stecha, Wood, & Fan, 2010). The method allows for high throughput screening, and comparison of different ligands regarding their efficacy and potency (Wolf, Takacs, Schmid, Lau, & Abbott, 2008). In GAL4-UAS-based LRAs, the ligand-binding domain (LBD) is utilized. The activity of the receptor is measured as light emitted, which corresponds to the activation of the receptor

as there is a fixed ratio between emitted photons and reacting substrate molecules (Branchini et al., 2018). The luciferase assay used in this study was a UAS/GAL4 system. The GAL4 system reduces potential interference from endogenous NRs present in the cell lines used. The overexpressed chimeric receptor also seems in general to be less toxic to the cells. Furthermore, with the GAL4-system, the activation of the receptor does not depend on the natural dimerization partner of the receptor tested (Chen, Xie, Agler, & Banks, 2003; Paguio et al., 2010).

GMPPARA2 MUTANTS WERE MORE SUSCEPTIBLE TO ACTIVATION BY WY-14643

WY-14643 is a well-known agonist for PPARa, which previously has been found to be one of the most potent exogenous ligands for PPARa in mammalian species (Bernardes et al., 2013; Peters, Cattley, & Gonzalez, 1997; J. Z. Zhang & Ward, 2010). Ppara in fish have also shown to be activated by WY-14643 (Laprairie, Denovan-Wright, & Wright, 2016; Leaver et al., 2005). The constructed mutants were hypothesized to have WY-14643 activation profiles more similar to those of gmPpara1, as the mutants had been changed to be more similar to this subtype. However, when the gmPpara2 mutants were exposed to WY-14643, an unprecedented strong increase in efficacy compared to the wt gmPparas was observed. The WY-14643-induced response (E_{max}) was significantly higher in cells expressing the constructed mutants compared to the wt gmPpara1 and gmPpara2. When comparing the activation profiles in more detail, the gmPpara2_DEL was significantly different from the three other constructed mutants (Table 4.4), where gmPpara2_DEL produced the highest efficacy (171-fold increase compared to unexposed cells, with an estimated EC_{50}=84.8 μM). For the mutants containing the substituted AAs in addition to the deletion, the fold activation differed between 134-145, but none of these were significantly different from each other (Table 4.3). The EC_{50} values were in the same range of gmPpar2_DEL, and estimated to be 85.5 μM, 79.6 μM and 92.3 μM, for gmPpara2_DEL_G>R+L>H, gmPpara2_DEL_G>R, and gmPpara2_DEL_L>H, respectively. These results show that the potencies of WY-14643 towards the constructed mutants were between the potency determined for gmPpara1 and gmPpara2 (Table 4.4 and 4.5), while the efficacy produced by WY-14643 was about 15 times higher than for gmPpara2, and 6 times higher than gmPpara1.

Notably, this demonstrates that removing the 14 AAs in the hinge region made a significant impact on the activation of the gmPpara2 receptor, especially with regard to efficacy. The higher efficacy of the gmPpara2_DEL mutation might be caused by structural or conformational changes in the receptor, potentially increasing its stability by shortening the predicted loop region between H1 and H3 as suggested by Bernandes et al (Bernardes et al., 2013). This loop extension is situated near both the ligand binding pocket and the coactivator binding site. Removal of this region may have increased the affinity of WY-14643. Moreover, the affinity of cofactors may also have been changed, where the AA deletion may have promoted the binding and recruitment of cellular cofactors. The mutants with additional AA substitutions seemed to have an opposite effect on the efficacy of WY-14643 than initially hypothesized, since the activation in these mutants were slightly reduced compared to the gmPpara2_DEL mutant. It must be emphasized that it is currently not known if this second binding site at all is capable of binding to WY-14643 in the gmPpara variants. As no increased efficacy or potency were observed when "restoring" this putative binding site in the gmPpar_DEL mutant, it may suggest that a second WY-14643 molecule is not recruited to this site. However, it cannot be excluded that binding of a second WY-14643 to this non-canonical binding site occurs, but the lowered efficacies are due to other conformational changes induced by the single AA mutations.

MUTATIONS DID NOT AFFECT SUSCEPTIBILITY TO PERFLUORINATED COMPOUNDS

Previously, it was shown that gmPpara1 could be activated by some PFASs, including PFOA and PFNA, but not gmPpara2. Because of time constraints only PFOA, PFNA and PFOS, were chosen to assess if the mutated gmPpara2 subtype could be activated by PFAS congeners. These three PFASs have also been most commonly used in the industries and consumer products (Jantzen et al., 2016).

The cytotoxicity of the PFASs used in the ligand activation assay was assessed for the COS-7 cells (Fig. 4.8). The metabolic activity was mostly reduced by PFOA (lowest 66 %), but also PFNA and PFOS showed some decrease in the metabolic activity. The membrane integrity was gradually reduced by all PFASs, and PFNA demonstrated the largest impact on the integrity. These effects may alter the ligand-activations in the LRA, potentially producing false low

luciferase activity when assessing for putative agonistic effects of the receptors. PFOA and PFOS were found to exert some cytotoxic effects in HepG2 cells (Florentin, Deblonde, Diguio, Hautemaniere, & Hartemann, 2011), but to a lesser extent than observed in this study. However, the cell lines are different (e.g. kidney vs. liver), which may contribute to the observed differences in the decrease in viability.

When the six different gmPpara variants were exposed to the PFAS molecules, PFOA and PFNA managed to activate gmPpara1 only. This activation of the wt gmPpara1 was as in line with previous findings. PFOA and PFNA produced a 7.6-fold and 2.7-fold activation of gmPpara1, respectively. For both the wt gmPpara2 and the constructed mutants, no activation of PFASs were observed. For PFOS, no activation was observed for any of the gmPparas, which also is in accordance with previous findings (S.Söderstrøm, 2017). These results suggest that removing the additional stretch of 14 AAs in the gmPpara2 hinge region does not affect the activation of gmPpara2s by PFASs *in vitro*. The hypothesis was that when the sequence of gmPpara2 became gradually more similar to gmPpara1, it would be activated by PFOA and PFNA. As this was not the case, it further indicates that neither the 14 AA deletion, nor the mutation of G278 and L286, were sufficient for constructing a PFAS-sensitive variant of gmPpara2.

Importantly, the mutations made in this study were not sufficient to provoke activation when the constructed mutants were exposed to selected PFASs. Hence, the reason for the different activation profiles must be attributed to differences located elsewhere in the protein structures. Importantly, there are still differences in the primary structures of gmPpara1 and gmPpara2 that were not assessed in this thesis. These are mainly single AA substitutions, but especially in the hinge region, such as from E190 to A199 in gmPpara1, there are larger stretches of AAs that differ between the two subtypes. Also, the region from V251 to G260 in gmPpara2 (Fig. 4.3), which is just before the extended region removed in this study, contains several AA differences that distinguish the two receptors. These may also contribute to the different activation profiles seen by the two subtypes. However, these differences were not investigated in this study.

CONCLUSION

Four different mutants, gmPpara2_DEL, gmPpara2_DEL_G>R, gmPpara2_DEL_L>H and gmPpara2_DEL_G>R+L>H, were successfully constructed to investigate the role of a 14 AA indel in the hinge region, and a putative secondary WY-14643 binding site, in the ligand activation of Atlantic cod gmPparas. When the gmPpara2 mutants were exposed to WY14643, the potencies were calculated to be between the EC_{50}-values determined for the two wt gmPparas. This means that the constructed mutants became more potent towards WY-14643. However, the efficacy, i.e. the fold activation produced by the gmPpara2 mutants, was higher than expected. The fold induction ranged between 134-171 for the different mutants, which was about 15 times higher than for wt gmPpara2, and 6 times higher than gmPpara1. This demonstrates that deleting the 14 AAs in gmPpar2 had the most impact on the activation profile, which may have increased the affinity towards WY-14643, or enhanced the stability of the receptor in an active conformation. The mechanistic and functional implications of the single AA mutations of the putative second binding for WY-14643 need to be elucidated further. Importantly, neither of the mutations performed affected the ability of gmPpara2 to be activated by PFASs.

FUTURE PERSPECTIVES

In this study some questions were answered, but many others were raised. For further studies *in silico* structure modeling and docking analysis of the constructed mutants when exposed to WY-14643 would be useful and helpful to understand why the mutants are more responsive than the wt gmPparas, while the potency is more consistent and in the range between gmPpara1 and gmPpara2. Recombinant expression and purification, followed by crystallization of the receptor mutants when bound to WY-14643 could be very useful. This could provide an understanding of why the mutants were so highly activated, which AAs are involved in the binding of WY-14643, how it is positioned in LBP, and if the predicted putative secondary binding site will bind WY-14643. Studying the gmPpara receptor exposed to WY-14643 and the selected PFASs with nuclear magnetic resonance (NMR) could also be useful, and provide more information regarding how the ligand binding occur, ligand binding affinities, stabilization and conformation of the protein structure, and the cofactor binding site.

In this thesis the extended region in the loop between H1 and H3 in gmPpara2 has been investigated and two AAs important for WY-14643 binding in the second allosteric binding site in hPPARa have been investigated in gmPpara2. There are still some sequence differences between gmPpara1 and gmPpara2. These changes can also be investigated and studied further with SDM to assess if they have an impact on both ligand binding of WY-14643 and the PFASs. More PFASs could also be included in the exposure, or a mixture of different PFASs could be used for exposure of the receptors in LRA to study if the PFASs activate differently, or activate in combination, or if they activate the receptor at all.

6. REFERENCES

Armstrong, C. T., Mason, P. E., Anderson, J. L. R., & Dempsey, C. E. (2016). Arginine side chain interactions and the role of arginine as a gating charge carrier in voltage sensitive ion channels. *Scientific Reports, 6*, 21759-21759. doi:10.1038/srep21759

Behr, A.-C., Plinsch, C., Braeuning, A., & Buhrke, T. (2020). Activation of human nuclear receptors by perfluoroalkylated substances (PFAS). *Toxicology in Vitro, 62*, 104700. doi:https://doi.org/10.1016/j.tiv.2019.104700

Bernardes, A., Souza, P. C. T., Muniz, J. R. C., Ricci, C. G., Ayers, S. D., Parekh, N. M., . . . Polikarpov, I. (2013). Molecular Mechanism of Peroxisome Proliferator-Activated Receptor α Activation by WY14643: a New Mode of Ligand Recognition and Receptor Stabilization. *Journal of molecular biology, 425*(16), 2878-2893. doi:https://doi.org/10.1016/j.jmb.2013.05.010

Bertrand, S., Thisse, B., Tavares, R., Sachs, L., Chaumot, A., Bardet, P.-L., . . . Laudet, V. (2007). Unexpected novel relational links uncovered by extensive developmental profiling of nuclear receptor expression. *PLoS genetics, 3*(11), e188-e188. doi:10.1371/journal.pgen.0030188

Billin, A. N. (2008). PPAR-β/δ agonists for Type 2 diabetes and dyslipidemia: an adopted orphan still looking for a home. *Expert Opinion on Investigational Drugs, 17*(10), 1465-1471. doi:10.1517/13543784.17.10.1465

Boisvert, G., Sonne, C., Rigét, F. F., Dietz, R., & Letcher, R. J. (2019). Bioaccumulation and biomagnification of perfluoroalkyl acids and precursors in East Greenland polar bears and their ringed seal prey. *Environmental Pollution, 252*, 1335-1343. doi:https://doi.org/10.1016/j.envpol.2019.06.035

Bopp, S. K., & Lettieri, T. (2008). Comparison of four different colorimetric and fluorometric cytotoxicity assays in a zebrafish liver cell line. *BMC pharmacology, 8*, 8-8. doi:10.1186/1471-2210-8-8

Branchini, B. R., Southworth, T. L., Fontaine, D. M., Kohrt, D., Florentine, C. M., & Grossel, M. J. (2018). A Firefly Luciferase Dual Color Bioluminescence Reporter Assay Using Two Substrates To Simultaneously Monitor Two Gene Expression Events. *Scientific Reports, 8*(1), 5990-5990. doi:10.1038/s41598-018-24278-2

Chen, T., Xie, W., Agler, M., & Banks, M. (2003). Coactivators in assay design for nuclear hormone receptor drug discovery. *Assay Drug Dev Technol, 1*(6), 835-842. doi:10.1089/154065803772613462

COMMISION, O. (2019, 07.09.2020). The OSPAR list of chemicals for priority action. Retrieved from https://www.ospar.org/work-areas/hasec/hazardous-substances/priority-action

Dale, K., Müller, M. B., Tairova, Z., Khan, E. A., Hatlen, K., Grung, M., . . . Goksøyr, A. (2019). Contaminant accumulation and biological responses in Atlantic cod (Gadus

morhua) caged at a capped waste disposal site in Kollevåg, Western Norway. *Marine Environmental Research, 145*, 39-51. doi:https://doi.org/10.1016/j.marenvres.2019.02.003

Den Broeder, M. J., Kopylova, V. A., Kamminga, L. M., & Legler, J. (2015). Zebrafish as a Model to Study the Role of Peroxisome Proliferating-Activated Receptors in Adipogenesis and Obesity. *PPAR Research, 2015*, 358029. doi:10.1155/2015/358029

Derosa, G., Sahebkar, A., & Maffioli, P. (2018). The role of various peroxisome proliferator-activated receptors and their ligands in clinical practice. *J Cell Physiol, 233*(1), 153-161. doi:10.1002/jcp.25804

Desvergne, B. a., & Wahli, W. (1999). Peroxisome Proliferator-Activated Receptors: Nuclear Control of Metabolism*. *Endocrine Reviews, 20*(5), 649-688. doi:10.1210/edrv.20.5.0380

Dreyer, C., Krey, G., Keller, H., Givel, F., Helftenbein, G., & Wahli, W. (1992). Control of the peroxisomal β-oxidation pathway by a novel family of nuclear hormone receptors. *Cell, 68*(5), 879-887. doi:https://doi.org/10.1016/0092-8674(92)90031-7

Eide, M., Rydbeck, H., Tørresen, O. K., Lille-Langøy, R., Puntervoll, P., Goldstone, J. V., . . . Karlsen, O. A. (2018). Independent losses of a xenobiotic receptor across teleost evolution. *Scientific Reports, 8*(1), 10404. doi:10.1038/s41598-018-28498-4

Fàbrega, F., Kumar, V., Schuhmacher, M., Domingo, J. L., & Nadal, M. (2014). PBPK modeling for PFOS and PFOA: Validation with human experimental data. *Toxicology Letters, 230*(2), 244-251. doi:https://doi.org/10.1016/j.toxlet.2014.01.007

Falandysz, J., Taniyasu, S., Yamashita, N., Rostkowski, P., Zalewski, K., & Kannan, K. (2007). Perfluorinated compounds in some terrestrial and aquatic wildlife species from Poland. *Journal of Environmental Science and Health, Part A, 42*(6), 715-719. doi:10.1080/10934520701304369

Florentin, A., Deblonde, T., Diguio, N., Hautemaniere, A., & Hartemann, P. (2011). Impacts of two perfluorinated compounds (PFOS and PFOA) on human hepatoma cells: Cytotoxicity but no genotoxicity? *International Journal of Hygiene and Environmental Health, 214*(6), 493-499. doi:https://doi.org/10.1016/j.ijheh.2011.05.010

Fujii, S., Polprasert, C., Tanaka, S., Hong Lien, N. P., & Qiu, Y. (2007). New POPs in the water environment: distribution, bioaccumulation and treatment of perfluorinated compounds – a review paper. *Journal of Water Supply: Research and Technology-Aqua, 56*(5), 313-326. doi:10.2166/aqua.2007.005

Germain, P., Staels, B., Dacquet, C., Spedding, M., & Laudet, V. (2006). Overview of nomenclature of nuclear receptors. *Pharmacol Rev, 58*(4), 685-704. doi:10.1124/pr.58.4.2

Gluzman, Y. (1981). SV40-transformed simian cells support the replication of early SV40 mutants. *Cell, 23*(1), 175-182. doi:10.1016/0092-8674(81)90282-8

Grygiel-Górniak, B. (2014). Peroxisome proliferator-activated receptors and their ligands: nutritional and clinical implications--a review. *Nutrition journal, 13*, 17-17. doi:10.1186/1475-2891-13-17

Guan, H.-P., Ishizuka, T., Chui, P. C., Lehrke, M., & Lazar, M. A. (2005). Corepressors selectively control the transcriptional activity of PPARgamma in adipocytes. *Genes & development, 19*(4), 453-461. doi:10.1101/gad.1263305

HGNC Guidelines. Retrieved from https://www.genenames.org/about/guidelines/

Hong, F., Xu, P., & Zhai, Y. (2018). The Opportunities and Challenges of Peroxisome Proliferator-Activated Receptors Ligands in Clinical Drug Discovery and Development. *International journal of molecular sciences, 19*(8), 2189. doi:10.3390/ijms19082189

Ingle, R. A. (2011). Histidine biosynthesis. *The arabidopsis book, 9*, e0141-e0141. doi:10.1199/tab.0141

Issemann, I., & Green, S. (1990). Activation of a member of the steroid hormone receptor superfamily by peroxisome proliferators. *Nature, 347*(6294), 645-650. doi:10.1038/347645a0

Issemann, I., & Green, S. (1990). Activation of a member of the steroid hormone receptor superfamily by peroxisome proliferators. *Nature, 347*(6294), 645-650. doi:10.1038/347645a0

Jantzen, C. E., Annunziato, K. A., Bugel, S. M., & Cooper, K. R. (2016). PFOS, PFNA, and PFOA sub-lethal exposure to embryonic zebrafish have different toxicity profiles in terms of morphometrics, behavior and gene expression. *Aquatic toxicology (Amsterdam, Netherlands), 175*, 160-170. doi:10.1016/j.aquatox.2016.03.026

Karlsen, O. A., Bjørneklett, S., Berg, K., Brattås, M., Bohne-Kjersem, A., Grøsvik, B. E., & Goksøyr, A. (2011). Integrative Environmental Genomics of Cod (Gadus morhua): The Proteomics Approach. *Journal of Toxicology and Environmental Health, Part A, 74*(7-9), 494-507. doi:10.1080/15287394.2011.550559

Kathuria, S. V., Chan, Y. H., Nobrega, R. P., Özen, A., & Matthews, C. R. (2016). Clusters of isoleucine, leucine, and valine side chains define cores of stability in high-energy states of globular proteins: Sequence determinants of structure and stability. *Protein science : a publication of the Protein Society, 25*(3), 662-675. doi:10.1002/pro.2860

Kliewer, S. A., Umesono, K., Noonan, D. J., Heyman, R. A., & Evans, R. M. (1992). Convergence of 9-cis retinoic acid and peroxisome proliferator signalling pathways through heterodimer formation of their receptors. *Nature, 358*(6389), 771-774. doi:10.1038/358771a0

Kota, B. P., Huang, T. H.-W., & Roufogalis, B. D. (2005). An overview on biological mechanisms of PPARs. *Pharmacological Research, 51*(2), 85-94. doi:https://doi.org/10.1016/j.phrs.2004.07.012

Laprairie, R. B., Denovan-Wright, E. M., & Wright, J. M. (2016). Subfunctionalization of peroxisome proliferator response elements accounts for retention of duplicated fabp1 genes in zebrafish. *BMC evolutionary biology, 16*(1), 147-147. doi:10.1186/s12862-016-0717-x

Leaver, M. J., Boukouvala, E., Antonopoulou, E., Diez, A., Favre-Krey, L., Ezaz, M. T., . . . Krey, G. (2005). Three Peroxisome Proliferator-Activated Receptor Isotypes from Each of Two Species of Marine Fish. *Endocrinology, 146*(7), 3150-3162. doi:10.1210/en.2004-1638

Liang, X., Gao, J., Li, D., & Cao, X. (2016). Cloning and expressions of peroxisome proliferator activated receptor alpha1 and alpha2 (PPARα1 and PPARα2) in loach (Misgurnus anguillicaudatus) and in response to different dietary fatty acids. *Biochemical and Biophysical Research Communications, 481*(1), 38-45. doi:https://doi.org/10.1016/j.bbrc.2016.11.022

Link, J. S., Bogstad, B., Sparholt, H., & Lilly, G. R. (2009). Trophic role of Atlantic cod in the ecosystem. *Fish and Fisheries, 10*(1), 58-87. doi:10.1111/j.1467-2979.2008.00295.x

Ma, X., Wang, D., Zhao, W., & Xu, L. (2018). Deciphering the Roles of PPARγ in Adipocytes via Dynamic Change of Transcription Complex. *Frontiers in endocrinology, 9*, 473-473. doi:10.3389/fendo.2018.00473

Maglich, J. M., Caravella, J. A., Lambert, M. H., Willson, T. M., Moore, J. T., & Ramamurthy, L. (2003). The first completed genome sequence from a teleost fish (Fugu rubripes) adds significant diversity to the nuclear receptor superfamily. *Nucleic acids research, 31*(14), 4051-4058. doi:10.1093/nar/gkg444

Metpally, R. P. R., Vigneshwar, R., & Sowdhamini, R. (2007). Genome inventory and analysis of nuclear hormone receptors in Tetraodon nigroviridis. *Journal of Biosciences, 32*(1), 43-50. doi:10.1007/s12038-007-0005-4

Muir, D., Bossi, R., Carlsson, P., Evans, M., De Silva, A., Halsall, C., . . . Roos, A. (2019). Levels and trends of poly- and perfluoroalkyl substances in the Arctic environment – An update. *Emerging Contaminants, 5*, 240-271. doi:https://doi.org/10.1016/j.emcon.2019.06.002

Nathan Dunn, D. H. (2019). *ZFIN Zebrafish Nomenclature Conventions*. Retrieved from https://wiki.zfin.org/display/general/ZFIN+Zebrafish+Nomenclature+Conventions

Ono, K., Knutsen, H., Olsen, E. M., Ruus, A., Hjermann, D. Ø., & Chr. Stenseth, N. (2019). Possible adverse impact of contaminants on Atlantic cod population dynamics in coastal ecosystems. *Proceedings of the Royal Society B: Biological Sciences, 286*(1908), 20191167. doi:10.1098/rspb.2019.1167

Pace, R. T., & Burg, K. J. L. (2015). Toxic effects of resazurin on cell cultures. *Cytotechnology, 67*(1), 13-17. doi:10.1007/s10616-013-9664-1

Paguio, A., Stecha, P., Wood, K. V., & Fan, F. (2010). Improved dual-luciferase reporter assays for nuclear receptors. *Current chemical genomics, 4*, 43-49. doi:10.2174/1875397301004010043

Patel, H., Truant, R., Rachubinski, R. A., & Capone, J. P. (2005). Activity and subcellular compartmentalization of peroxisome proliferator-activated receptor α are altered by the centrosome-associated protein CAP350. *Journal of Cell Science, 118*(1), 175. doi:10.1242/jcs.01600

Peters, J. M., Cattley, R. C., & Gonzalez, F. J. (1997). Role of PPAR alpha in the mechanism of action of the nongenotoxic carcinogen and peroxisome proliferator Wy-14,643. *Carcinogenesis, 18*(11), 2029-2033. doi:10.1093/carcin/18.11.2029

Petrat, F., Boengler, K., Schulz, R., & de Groot, H. (2012). Glycine, a simple physiological compound protecting by yet puzzling mechanism(s) against ischaemia-reperfusion injury: current knowledge. *British journal of pharmacology, 165*(7), 2059-2072. doi:10.1111/j.1476-5381.2011.01711.x

Prevedouros, K., Cousins, I. T., Buck, R. C., & Korzeniowski, S. H. (2006). Sources, Fate and Transport of Perfluorocarboxylates. *Environmental Science & Technology, 40*(1), 32-44. doi:10.1021/es0512475

Söderstrøm, Sofie. (2017). *Peroxisome Proliferator-Activated Receptors (PPARs) As Tools For Studying Effects Of Contaminants On The Lipid Metabolism In Atlantic Cod (Gadus morhua)*. MSc thesis, Department of Biology, Environmental Toxicology. University of Bergen.

Schlezinger, J. J., Puckett, H., Oliver, J., Nielsen, G., Heiger-Bernays, W., & Webster, T. F. (2020). Perfluorooctanoic acid activates multiple nuclear receptor pathways and skews expression of genes regulating cholesterol homeostasis in liver of humanized PPARα mice fed an American diet. *bioRxiv*, 2020.2001.2030.926642. doi:10.1101/2020.01.30.926642

Schreer, A., Tinson, C., Sherry, J. P., & Schirmer, K. (2005). Application of Alamar blue/5-carboxyfluorescein diacetate acetoxymethyl ester as a noninvasive cell viability assay in primary hepatocytes from rainbow trout. *Analytical Biochemistry, 344*(1), 76-85. doi:https://doi.org/10.1016/j.ab.2005.06.009

Schultes, L., Sandblom, O., Broeg, K., Bignert, A., & Benskin, J. P. (2020). Temporal Trends (1981-2013) of Per- and Polyfluoroalkyl Substances and Total Fluorine in Baltic cod (Gadus morhua). *Environmental toxicology and chemistry, 39*(2), 300-309. doi:10.1002/etc.4615

Shang, J., Brust, R., Mosure, S. A., Bass, J., Munoz-Tello, P., Lin, H., . . . Kojetin, D. J. (2018). Cooperative cobinding of synthetic and natural ligands to the nuclear receptor PPARγ. *eLife, 7*, e43320. doi:10.7554/eLife.43320

Simonnet-Laprade, C., Budzinski, H., Maciejewski, K., Le Menach, K., Santos, R., Alliot, F., . . . Labadie, P. (2019). Biomagnification of perfluoroalkyl acids (PFAAs) in the food

web of an urban river: assessment of the trophic transfer of targeted and unknown precursors and implications. *Environmental Science: Processes & Impacts, 21*(11), 1864-1874. doi:10.1039/C9EM00322C

Söderstrøm, Sofie, Roger Lille-Langøy, Fekadu Yadetie, Annick Dejaegere, Roland Stote, Anders Goksøyr and Odd André Karlsen. (2020). *Agonistic and potentiating effects of perfluoroalkyl substances on the Atlantic cod (Gadus morhua) peroxisome proliferator-activated receptors*. Manuscrpit in prep. Department of Biological Sciences, Integrated Structural Biology Department. University of Bergen, Norway, Integrated Structural Biology Department, University of Strasbourg, France.

Star, B., Nederbragt, A. J., Jentoft, S., Grimholt, U., Malmstrøm, M., Gregers, T. F., . . . Jakobsen, K. S. (2011). The genome sequence of Atlantic cod reveals a unique immune system. *Nature, 477*(7363), 207-210. doi:10.1038/nature10342

Takacs, M. L., & Abbott, B. D. (2007). Activation of Mouse and Human Peroxisome Proliferator–Activated Receptors (α, β/δ, γ) by Perfluorooctanoic Acid and Perfluorooctane Sulfonate. *Toxicological Sciences, 95*(1), 108-117. doi:10.1093/toxsci/kfl135

Tyagi, S., Gupta, P., Saini, A. S., Kaushal, C., & Sharma, S. (2011). The peroxisome proliferator-activated receptor: A family of nuclear receptors role in various diseases. *Journal of advanced pharmaceutical technology & research, 2*(4), 236-240. doi:10.4103/2231-4040.90879

Valdersnes, S., Nilsen, B. M., Breivik, J. F., Borge, A., & Maage, A. (2017). Geographical trends of PFAS in cod livers along the Norwegian coast. *PLoS ONE, 12*(5), e0177947-e0177947. doi:10.1371/journal.pone.0177947

Waterhouse, A. M., Procter, J. B., Martin, D. M., Clamp, M., & Barton, G. J. (2009). Jalview Version 2--a multiple sequence alignment editor and analysis workbench. *Bioinformatics, 25*(9), 1189-1191. doi:10.1093/bioinformatics/btp033

Werman, A., Hollenberg, A., Solanes, G., Bjorbaek, C., Vidal-Puig, A. J., & Flier, J. S. (1997). Ligand-independent activation domain in the N terminus of peroxisome proliferator-activated receptor gamma (PPARgamma). Differential activity of PPARgamma1 and -2 isoforms and influence of insulin. *J Biol Chem, 272*(32), 20230-20235. doi:10.1074/jbc.272.32.20230

Wolf, C. J., Takacs, M. L., Schmid, J. E., Lau, C., & Abbott, B. D. (2008). Activation of Mouse and Human Peroxisome Proliferator−Activated Receptor Alpha by Perfluoroalkyl Acids of Different Functional Groups and Chain Lengths. *Toxicological Sciences, 106*(1), 162-171. doi:10.1093/toxsci/kfn166

Xu, H. E., Lambert, M. H., Montana, V. G., Plunket, K. D., Moore, L. B., Collins, J. L., . . . Willson, T. M. (2001). Structural determinants of ligand binding selectivity between the peroxisome proliferator-activated receptors. *Proceedings of the National Academy of Sciences, 98*(24), 13919. doi:10.1073/pnas.241410198

Yadetie, F., Bjørneklett, S., Garberg, H. K., Oveland, E., Berven, F., Goksøyr, A., & Karlsen, O. A. (2016). Quantitative analyses of the hepatic proteome of methylmercury-exposed Atlantic cod (Gadus morhua) suggest oxidative stress-mediated effects on cellular energy metabolism. *BMC Genomics, 17*, 554-554. doi:10.1186/s12864-016-2864-2

Yadetie, F., Oveland, E., Døskeland, A., Berven, F., Goksøyr, A., & Karlsen, O. A. (2017). Quantitative proteomics analysis reveals perturbation of lipid metabolic pathways in the liver of Atlantic cod (Gadus morhua) treated with PCB 153. *Aquatic Toxicology, 185*, 19-28. doi:https://doi.org/10.1016/j.aquatox.2017.01.014

Zhang, H. X., Du, G. H., & Zhang, J. T. (2004). Assay of mitochondrial functions by resazurin in vitro. *Acta Pharmacol Sin, 25*(3), 385-389.

Zhang, J. Z., & Ward, K. W. (2010). WY-14 643, a selective PPAR{alpha} agonist, induces proinflammatory and proangiogenic responses in human ocular cells. *Int J Toxicol, 29*(5), 496-504. doi:10.1177/1091581810376674

Zhang, W., Sakai, T., Fujiwara, S., & Hatano, Y. (2017). Wy14643, an agonist for PPARα, downregulates expression of TARC and RANTES in cultured human keratinocytes. *Experimental Dermatology, 26*(5), 457-459. doi:10.1111/exd.13245

Zoete, V., Grosdidier, A., & Michielin, O. (2007). Peroxisome proliferator-activated receptor structures: Ligand specificity, molecular switch and interactions with regulators. *Biochimica et Biophysica Acta (BBA) - Molecular and Cell Biology of Lipids, 1771*(8), 915-925. doi:https://doi.org/10.1016/j.bbalip.2007.01.007

APPENDIX

Functional Characterization of Atlantic Cod (*Gadus morhua*) Peroxisome Proliferator-activated Receptor alpha 1 and alpha 2

Kristianne Hjorth Viken[1], Roger Lille-Langøy[1], Anders Goksøyr[1], Odd André Karlsen[1]
[1] Department of Biological Sciences, University of Bergen, Norway

Kristianne Hjorth Viken
University of Bergen
Krisitanne.Viken@student.uib.no

Background and aims

Atlantic cod (*Gadus morhua*) has four paralogous peroxisome proliferator-activated receptors (Ppars), including Ppar alpha 1 and 2, Ppar beta/delta, and Ppar gamma. Ppars are ligand activated transcription factors that are members of the superfamily of nuclear receptors. The different Ppars have important, but distinct, roles in energy metabolism (1, 2). Previously, we have demonstrated that gmPpara1 could be activated by some exogenous compounds, including the hsPPARA model-agonist WY-14643, and the perfluoralkylated substances (PFASs) PFHxA, PFOA, PFNA and PFHxS. gmPpara2 were also activated by WY-14643, but none of the PFASs (2).

The protein sequences of gmPpara1 and gmPpara2 have some important differences. The gmPpara2 has an insertion of 14 amino acids in the hinge region. In addition, two of the amino acids important for binding of WY-14643 in a second "allosteric" binding site are also changed in gmPpara2. We hypothesize that these differences cause the observed discrepancies in the activation profiles of gmPpara1 and gmPpara2. In this study gmPpara2 has been mutated to become structurally more similar to gmPpara1, and a luciferase reporter gene assay (LRA) has been used to assess ligand activation of the produced Ppara2 mutants.

Methods

Site-directed mutagenesis (SDM) was used to obtain the desired mutants of gmPpara2, and LRA was used to measure the receptor activity when exposed to the ligand WY-14643. When doing SDM, first the insertion in gmPpara2 was deleted, then the single amino acid mutations were done on the first constructed mutant.

Workflow

Site-Directed Mutagenesis of Ppara2 → Luciferase Reporter Gene Assay with Ppara2 mutants

Luciferase reporter gene assay

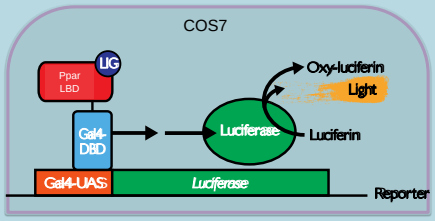

Figure 1: **Workflow and methods.** GAL4-DBD/UAS based reporter gene assay with the Ppar ligand binding domain. Activation of Ppar by a ligand (LIG), which promotes transcription of the luciferase gene. The luciferase protein converts the substrate luciferin to oxyluciferin, in a reaction that produces light that can be measured with a luminometer.

Results and discussion

SDM produced the desired mutants, as can be seen in the multiple sequence alignment (Figure 2). The activation profiles of gmPpara1 and gmPpara2 wild types and mutants with the WY-14643 ligand were assessed with the LRA (Figure 3). The EC_{50} and E_{max} of the the different mutants were estimated from a dose-response curve generated by non-linear regression using GraphPad Prism 7.0 (Table 1).

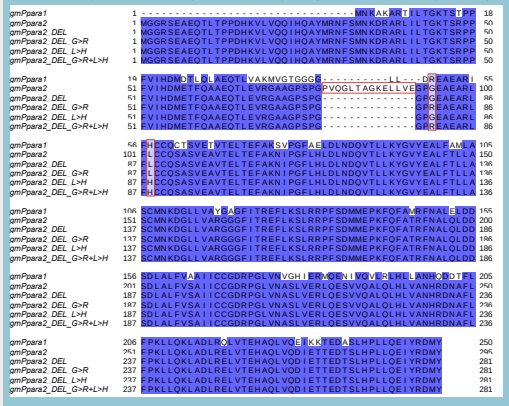

Figure 2: Multiple sequence alignment of the protein sequences of the wild type and mutated gmPpars. Insertion and single amino acid mutations are marked in red.

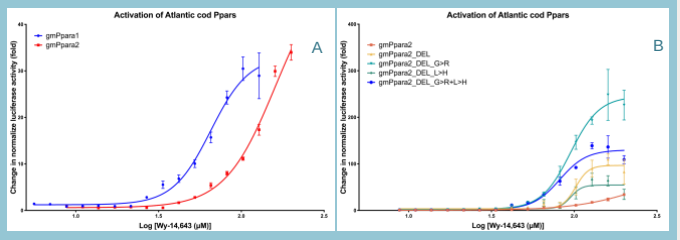

Figure 3: Activation profiles of the wild type gmPpars (A) and gmaPpara2 mutants (B) when exposed to WY-14634. WY-14643 structure is shown.

Receptor	gmPpara1	gmPpara2	gmPpara2_ DEL	gmPpara2_ DEL_G>R	gmPpara2_ DEL_L>H	gmPpara2_ DEL_G>R+L>H
EC_{50} (µM)	88.0	116.0	121.4	115.5	71.6	81.7
E_{max} (fold)	45.3	33.4	179.7	204.0	74.0	127.6

Table 1: Potency and efficacy of gmPparas exposed to WY-14643. EC_{50} and E_{max} values for gmPpars exposed to WY-14643 are shown.

Conclusions and further work

All the gmPpara2 mutants were shown to be activated by the known agonist WY-14643. Preliminary results indicates that the deletion of the 14 AA increase the efficacy but not the potency of the WY-14,643 response. The G93R substitution appear to slightly increase the efficacy, while the L102H substitution appear to lower efficacy and increase potency. More experiments are needed to obtain enough data for statistical analysis. Further work include to study if the substitution and/or amino acids 93 and 57 explain the observed differences in responses of gmPpara1 and gmPara2 exposed to PFASs.

REFERENCES 1. Tyagi et.al. (2011) J Adv Pharm Tech Res 2. S. Söderström (2017) Environmental Toxicology

ACKNOWLEDGEMENTS
This study is part of iCod 2.0: Integrative environmental genomics of Atlantic cod funded by the Research Council of Norway (project no. 244564) and dCod 1.0 project funded by the Research Council of Norway (project no. 248840) as part of the Digital Life Norway initiative.

dCod 1.0 decoding the systems toxicology of atlantic cod

UNIVERSITY OF BERGEN